# Preparation and Characterization of Amorphous Ciprofloxacin-Amino Acid Salts

Hanah Mesallati[a], Daryl Conroy[a], Sarah Hudson[b], Lidia Tajber[a,*]

[a]Synthesis and Solid State Pharmaceutical Centre, School of Pharmacy and Pharmaceutical Sciences, Trinity College Dublin, College Green, Dublin 2, Ireland.

[b]Synthesis and Solid State Pharmaceutical Centre, Department of Chemical Sciences, Bernal Institute, University of Limerick, Castletroy, Limerick, Ireland.

[*]Corresponding author. School of Pharmacy and Pharmaceutical Sciences, Trinity College Dublin, College Green, Dublin 2, Ireland. Tel: +35318962787. Email address: ltajber@tcd.ie.

**Abstract**

The amorphization of the poorly soluble drug ciprofloxacin (CIP) may be facilitated by the use of a suitable stabilizer. In this study seven amino acids, with various side chain properties, were evaluated in this regard. Solid dispersions were prepared by ball milling 1:1 molar ratios of CIP with the amino acids, and their solid-state and pharmaceutical properties were then examined. Fully X-ray amorphous solid dispersions were obtained with aspartic acid, glutamic acid, cysteine and arginine. In each case, evidence of salt formation between the drug and amino acids was found via Fourier transform infrared spectroscopy and solid-state nuclear magnetic resonance. In contrast, semi-crystalline solid dispersions were obtained with serine, alanine and glycine. The glass transition temperatures of the amorphous salts were significantly higher than those of the starting materials, and they remained fully X-ray amorphous during long-term stability studies. Significant improvements in the solubility of CIP were also observed with the amorphous salts in water and simulated biological fluids, over and above that of the corresponding physical mixtures. In permeability studies on the other hand, the amorphous aspartate and glutamate salts were found to be less permeable than the pure drug, whereas formulation as an amorphous salt containing cysteine or arginine increased the permeability of CIP. Therefore, while amorphous salt formation with amino acids appears to be a suitable means of improving the thermal stability and solubility of CIP, in some cases this is associated with a decrease in permeability.

**Keywords:** Ciprofloxacin, amorphous salt, amino acid, ball milling, stability, solubility, permeability.

**Abbreviations:** ASD, amorphous solid dispersion; CIP, ciprofloxacin; PM, physical mixture; SD, semi-crystalline solid dispersion.

## 1. Introduction

Ciprofloxacin (CIP) is a class IV Biopharmaceutics Classification System (BCS) drug [1]. It usually exists in the zwitterionic form in the solid state, with a positively charged piperazine amino group and negatively charged carboxylate group (Fig. 1). These charged groups participate in extensive intermolecular interactions, resulting in a stable crystal lattice [2]. Unfortunately, this contributes to the poor solubility of this drug, which is equal to 0.09 mg/mL in water at 37 $^{o}$C [3].

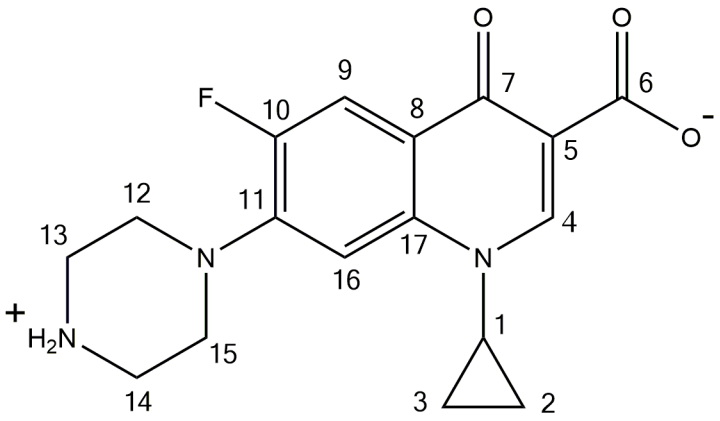


**Fig. 1.** Chemical structure of ciprofloxacin, with carbon atoms numbered.

For drugs with solid-state limited solubility such as CIP, salt formation, amorphization, or a combination of these approaches may be used to improve their solubility [4]. However, due to its stable crystal lattice, CIP is a difficult drug to amorphize. In addition, its low solubility and thermal degradation limit the methods available to amorphize it. In a recent study, only spray drying in pure water was found to produce the fully X-ray amorphous form of the pure drug; however, this was a very inefficient process in terms of production yield [2].

Although amorphous solids are more soluble than their crystalline counterparts, a major limitation to their widespread use is their low physical stability. This may be improved by the production of amorphous solid dispersions (ASDs) using various excipients. ASDs may contain polymers or small molecules, although the latter are often referred to as co-amorphous formulations to distinguish them from polymeric systems [5]. The production of a number of CIP ASDs via ball milling was recently described by our group. Only acidic polymers were successful in this regard, and in each case an ionic interaction between the positively charged piperazine amino group of CIP and carboxylate groups of the polymers was detected. The ASDs were found to have higher than expected $T_g$'s and remained stable when exposed to high humidity, while also demonstrating improved solubility in water and simulated intestinal fluid [3]. Amorphous CIP/succinic acid salts have also been prepared by ball milling and spray drying. These salts improved the aqueous solubility of CIP by over 300 times, however they were unstable when exposed to water [6].

Recently, a number of studies have focused on amorphous formulations consisting of poorly soluble drugs and amino acids. Amino acids are attractive co-formers for such formulations as they are inexpensive GRAS (generally recognized as safe) compounds [7], that have been shown to improve the physical stability of many amorphous drugs [8–11]. The α-carboxylate, α-amino group or side chains of amino acids can all potentially form bonds with drugs, providing many possibilities in terms of intermolecular interactions. Amino acids may stabilize amorphous drugs via hydrogen bonding, hydrophobic and/or ionic interactions [7], however amorphous formulations that lack specific drug-amino acid interactions have also been produced [8]. A number of amorphous salts have been prepared with the basic amino acids, in particular arginine (ARG), via ball milling and spray drying [9,12,13]. In each of these salts an ionic interaction

between the positively charged side chain guanidyl group of ARG and a carboxylate group of the drug was detected [8,12,13].

From previous work with CIP, it could be predicted that successful amorphization of the drug would be most likely with the acidic amino acids, i.e. aspartic acid (ASP) and glutamic acid (GLU). A study by Elshaer et al supports this hypothesis. The authors found that CIP formed salts with ASP and GLU when freeze dried in a 1:1 molar ratio [14]. In both cases the positively charged piperazine amino group of CIP was found to form an ionic interaction with a carboxylate group of ASP and GLU. In contrast, the authors were unable to form salts with the basic amino acids arginine, lysine and histidine [14]. Similarly, when CIP was milled with neutral polymers, such as PVP and Soluplus, a semi-crystalline product was obtained [3]. However, since all amino acids contain an α-carboxyl group, they are more likely to interact with the amino group of CIP, and potentially form an amorphous salt, than such polymers.

The major goal of this study was to explore the possibility of forming amorphous formulations containing CIP and amino acids. Seven amino acids with differing side chain properties were chosen for analysis: glycine (GLY), alanine (ALA), serine (SER), arginine (ARG), cysteine (CYS), glutamic acid (GLU) and aspartic acid (ASP). Their chemical structures are shown in Fig. 2. Their side chains, or R groups, may be classified as nonpolar and aliphatic (GLY and ALA); polar and uncharged (SER and CYS); basic (ARG); and acidic (ASP and GLU). Solid dispersions were produced by ball milling CIP with the amino acids in a 1:1 molar ratio. Powder X-ray diffraction (PXRD), differential scanning calorimetry (DSC), Fourier transform infrared spectroscopy (FTIR) and solid-state nuclear magnetic resonance (SSNMR) were used to detect the physical form and thermal behavior of the preparations, and the interactions between the

components. The long-term stability of the successful amorphous formulations, as well as the effect of water sorption on their physical state, was then examined.

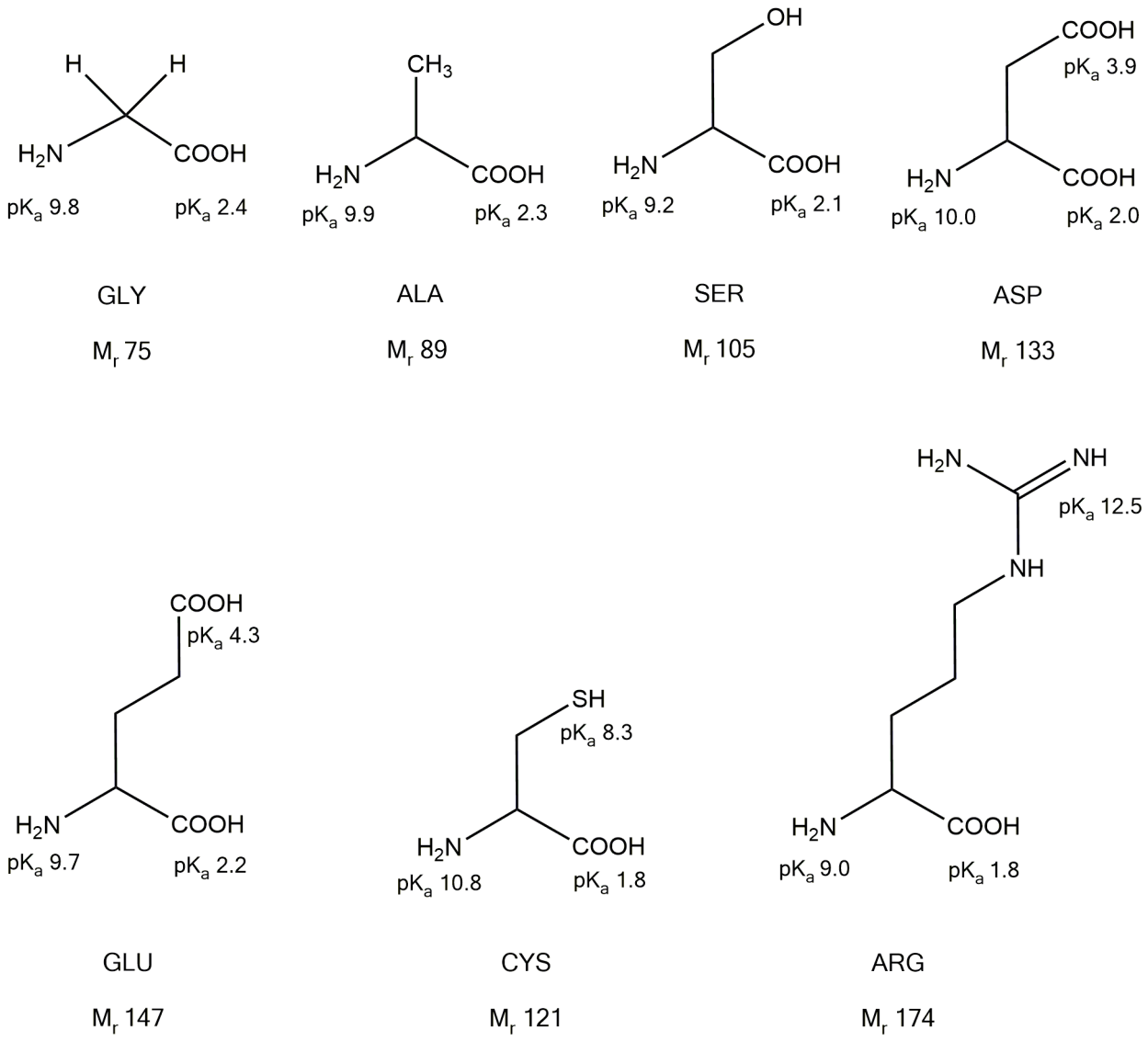


**Fig. 2.** Chemical structures, $pK_a$ values and molecular weights of the amino acids used in this study.

The solubility and dissolution rate of a range of poorly soluble drugs have been found to increase via the production of amorphous amino acid formulations [8,10,15], while the CIP aspartate and

glutamate salts prepared by Elshaer et al were significantly more soluble in water than crystalline CIP [14]. It was therefore of interest to determine whether this is also the case with the amorphous samples prepared in this study. However, it is important to remember that the solubility and permeability of a substance are closely linked, with an increase in one property commonly associated with a decrease in the other [16]. The effective permeability of the amorphous samples was therefore compared to that of pure crystalline CIP using the parallel artificial membrane permeability assay (PAMPA).

## 2. Materials and Methods

### 2.1. Materials

Ciprofloxacin (CIP) was obtained from Carbosynth Limited, Berkshire, U.K. Ciprofloxacin hydrochloride salt (CIP HCl) was kindly donated by Hemofarm, Serbia. The following amino acids were used to form solid dispersions with CIP: glycine (GLY: Sigma-Aldrich, St. Louis), L-alanine (ALA: Acros Organics, New Jersey), L-cysteine (CYS: SAFC, Sigma-Aldrich, St. Louis), L-serine (SER: Acros Organics, New Jersey), L-arginine (ARG: Sigma-Aldrich, St. Louis), L-glutamic acid (GLU: Acros Organics, New Jersey) and L-aspartic acid (ASP: Sigma-Aldrich, Dorset). The PXRD patterns of the starting materials are shown in Fig. A.1a, Supplementary Material.

Fasted state simulated gastric fluid (FaSSGF) was produced by adding 60 mg SIF® Powder Original (biorelevant.com, Surrey, U.K.) to one liter of FaSSGF HCl solution, consisting of 34 mM NaCl adjusted to pH 1.6 with HCl. Fasted state simulated intestinal fluid (FaSSIF) was

produced by adding 2.24 g SIF® Powder Original to one liter of FaSSIF phosphate buffer, consisting of 19.5 mM NaOH, 25 mM $NaH_2PO_4.H_2O$ and 106 mM NaCl, adjusted to pH 6.5 with NaOH. NaOH pellets were obtained from Riedel-de Haën, Seelze, Germany, $NaH_2PO_4.H_2O$ from Merck, Darmstadt, Germany and NaCl from Sigma-Aldrich Ireland Ltd., Arklow, Ireland. Triethylamine, dodecane, lecithin (L-α-phosphatidylcholine, Type XVI-E) and phosphate buffered saline (PBS) tablets were obtained from Sigma-Aldrich Ireland Ltd., Arklow, Ireland. All other chemicals and solvents were of analytical grade.

### 2.2. Sample Preparation

Ball milling was carried out at room temperature (RT) using a Retsch planetary ball mill PM 100 (Haan, Germany). 2 g of powder was added to 50 mL stainless steel grinding bowls. Three stainless steel milling balls of 20 mm diameter and 32 g weight were used. The amino acids were first ball milled individually for 4 hours. CIP was then co-milled with the amino acids in a 1:1 molar ratio. The powder mixtures were each milled for 4–6 hours in total, in intervals of 15 min with 10 min breaks in between. At 1, 2, 4 and 6 hours, small samples of powder were taken for analysis by powder X-ray diffraction. Physical mixtures (PMs) were prepared by mixing "as received" CIP and the amino acid powders in a pestle and mortar for a few minutes. The PXRD patterns of the PMs are shown in Fig. A.1b, Supplementary Material.

### 2.3. Solid State Characterization

#### 2.3.1. Powder X-ray Diffraction (PXRD)

PXRD was carried out at RT using a benchtop Rigaku MiniflexII X-ray diffractometer (Tokyo, Japan) and a Haskris cooler (Illinois, USA). The samples were scanned from 5 to 40 2θ degrees in steps of 0.05. A scan rate of 0.05º per second and signal collection time of 1 s per step were used. The tube (Cu, 1 kW normal focus) had an output voltage and current of 30 kV and 15 mA, respectively.

### 2.3.2. Fourier Transform Infrared Spectroscopy (FTIR)

FTIR was performed using a Spectrum One FT-IR Spectrometer (Perkin Elmer, Connecticut, USA) equipped with Spectrum Software version 6.1. A spectral range of 450–4000 $cm^{-1}$, resolution of 4 $cm^{-1}$, scan number of 10 and scan speed of 0.2 cm/s were used. KBr disks were produced by direct compression, using a pressure of approximately 1 MPa for 1 min. A sample loading of 1% (w/w) was used.

### 2.3.3. Solid-State Nuclear Magnetic Resonance (SSNMR)

Carbon-13 NMR spectra were acquired on a Bruker Avance III HD NMR spectrometer operating at $B_0$ = 9.4 T, with corresponding $^{1}H$ and $^{13}C$ resonance frequencies of $\nu_0(^{1}H)$ = 400.1 MHz and $\nu_0(^{13}C)$ = 100.6 MHz. Samples were packed in 4 mm outer diameter zirconia rotors with Kel-F caps under ambient atmosphere, and experimental $^{13}C$ NMR spectra were acquired at natural abundance using a 4 mm triple channel (H/X/Y) Bruker MAS probe operating in double resonance mode. The magic angle was optimized using a rotor packed with KBr and spun at 5 kHz. NMR spectra were referenced to TMS at $\delta_{iso}$ = 0 ppm by setting the high frequency $^{13}C$ resonance in adamantane to 38.48 ppm [17]. The $^{13}C$ CP/MAS NMR spectra were acquired in a single spectral window using the cross-polarization pulse sequence, with a magic angle spinning (MAS) rotor frequency of 10 kHz, a $^{1}H$ 90° pulse width of 2.5 μs, and 50 kHz $^{1}H$ decoupling

during acquisition. Proton decoupling was carried out with the SPINAL64 [18] decoupling sequence at 100%. A contact time of 2.5 ms was optimized using a crystalline sample of CIP and was used for the acquisition of all $^{13}C$ CP/MAS NMR spectra. Recycle delays were varied from 5 s (more amorphous samples) to 20 s (more crystalline samples), depending on the measured $^{1}H$ $T_1$ relaxation time for each sample. For each sample, the $^{1}H$ $T_1$ relaxation time(s) were checked using the saturation recovery pulse sequence to ensure that the recycle delay allowed for adequate relaxation between the collection of subsequent transients. The NMR spectra varied from 128 to 4k transients, with more transients being collected for the amorphous samples to get a suitable signal to noise ratio. Samples were dried overnight in an oven at 50 °C prior to SSNMR analysis.

### 2.3.4. Differential Scanning Calorimetry (DSC)

DSC was carried out using a Mettler Toledo DSC (Schwerzenbach, Switzerland). The purge gas was nitrogen. Approximately 5–10 mg samples were analyzed in sealed 40 µL aluminum pans with pierced lids. In order to elucidate the glass transition temperature ($T_g$) of the ASDs, the samples were first heated from 25 to 70 ºC to remove any water present in the powder. When cool, the samples were reheated from 25 to 300 ºC at a rate of 10 ºC/min. All measurements were carried out in triplicate. The thermograms were analyzed using Mettler Toledo STARe software (version 6.10). The midpoint of the transition was taken as the $T_g$.

### 2.3.5. High-Speed Differential Scanning Calorimetry (HSDSC)

HSDSC was carried out on all of the ball milled CIP/amino acid samples with a PerkinElmer Diamond DSC (Waltham, MA, USA) with a ULSP B.V. 130 cooling system (Ede, Netherlands). A helium gas flow of 60 mL/min was controlled with a PerkinElmer Thermal Analysis Gas

Station. The instrument was calibrated using indium and zinc standards. Approximately 3–5 mg samples were analyzed in 18 µL aluminum pans sealed with aluminum lids. The samples were first heated from 25–80 °C and cooled to 5 °C to allow for water evaporation. They were then heated from 5–300 °C with a heating rate of 50–300 °C/min.

### 2.3.6. Thermogravimetric Analysis (TGA)

TGA was carried out on the ASDs using a Mettler TG50 measuring module coupled to a Mettler Toledo MT5 balance (Schwerzenbach, Switzerland). Approximately 8–10 mg samples were analyzed in open aluminum pans, using nitrogen as the purge gas. Samples were heated from 25 to 300 °C at a rate of 10 °C/min. Mettler Toledo STARe software (version 6.10) was used to analyze the thermograms.

## 2.4. Ciprofloxacin Aspartate and Glutamate Crystallization

1:2 molar ratio solutions of CIP and ASP or GLU were prepared in a mixture of ethanol and water (approximately 3:1 volume ratio) at a concentration of 1% (w/v). These solutions were allowed to evaporate slowly at RT. When dry, the crystals were analyzed by PXRD. A portion of the ball milled CIP/ASP and CIP/GLU amorphous formulations were also left exposed at RT (22–25 °C) for a number of months to encourage their crystallization. The samples were analyzed regularly by PXRD.

## 2.5. Dynamic Vapor Sorption (DVS)

DVS studies were carried out using an Advantage-1 automated gravimetric vapor sorption analyzer (Surface Measurement Systems Ltd., London, U.K.). The temperature was maintained at 25.0 ± 0.1 °C. Approximately 10 mg samples were added to the sample basket and placed in

the instrument. These were equilibrated at 0% relative humidity (RH) until a constant mass was obtained (dm/dt ≤ 0.002 mg/min). The reference mass was recorded and sorption-desorption analysis was then carried out between 0 and 90% RH, in steps of 10% RH. At each stage, the sample mass was equilibrated (dm/dt ≤ 0.002 mg/min for at least 10 min) before the RH was changed. An isotherm was calculated from the complete sorption and desorption profile. Following DVS analysis the samples were analyzed by PXRD. DVS was repeated on fresh samples under the same conditions, however they were removed for PXRD analysis upon crystallization during the sorption cycle.

### 2.6. Long-Term Stability Study

The CIP/amino acid ASDs were stored at RT (22–25 $^{o}$C) under dry storage conditions in a desiccator (silica gel). Samples of each powder were taken at regular intervals for a period of 12 months. PXRD was used to determine whether crystallization had occurred in any of the samples.

### 2.7. Dynamic Solubility Studies

5–10 mL of water, FaSSGF or FaSSIF were added to 40 mL glass vials. These were placed into jacketed beakers connected to a Lauda M12 waterbath (Lauda-Königshofen, Germany) and allowed to equilibrate to 37 $^{o}$C. A quantity of sample in excess of its expected saturated solubility was added to the stirred vials. Aliquots were drawn from the vials at specific time points over a 2 hour period, and filtered with 0.45 µm PTFE membrane filters (VWR, USA). The filtered solutions were then diluted with a 2.45 g/L solution of phosphoric acid, previously adjusted to pH 3.0 with triethylamine. The concentration of CIP in each of the diluted samples was measured by HPLC. The solubility studies were repeated at least in triplicate with each

medium. The pH of the solutions was measured before the addition of the samples and at the end of the 2 hour study using a Thermo Orion 420A+ pH meter (Thermo Scientific, Hampshire, U.K.). The solid material left in the vials at the end of the studies was filtered and analyzed by PXRD.

### 2.8. Parallel Artificial Membrane Permeability Assay (PAMPA)

Permeability studies were carried out using the lipid-PAMPA method described previously [3]. A 96-well MultiScreen Filter Plate, with underdrain removed, was used as the donor plate, and a 96-well MultiScreen Transport Receiver Plate as the acceptor plate (Millipore Corporation, Billerica, MA, USA). Samples were dissolved in pH 7.4 PBS at a concentration of 50–100 µg/mL. 300 µL of PBS pH 7.4 was added to each well of the acceptor plate. 5 µL of a 1% (w/v) solution of lecithin in dodecane was added to the filter within each donor well to form an artificial membrane. 150 µL of the sample solutions were immediately added to each well of the donor plate in triplicate. The donor plate was then placed into the acceptor plate and incubated at RT for 16 hours. Following incubation, the contents of each well in the acceptor plate was diluted 1:4 with HPLC mobile phase and filtered with 0.45 µm PTFE membrane filters (VWR, USA). The concentration of CIP in each sample was then measured using HPLC.

The effective permeability ($P_e$) of the samples was calculated using the following equation [19]:

$$P_e = -\ln(1 - r)\left(\frac{V_D V_A}{(V_D+V_A)At}\right) \text{ where } r = \frac{[\text{Drug}]_{\text{Acceptor}}}{[\text{Drug}]_{\text{Equilibrium}}} \quad (1)$$

$V_D$ and $V_A$ are the volumes of the donor and acceptor compartment, respectively, in $cm^3$, t is the incubation time in seconds, and A is the active surface area of the membrane (equal to the membrane area multiplied by the porosity ratio. For Millipore MultiScreen Permeability Filter

Plate membranes this is equal to 0.24 $cm^2$ x 100%, or 0.24 $cm^2$) [20]. $[Drug]_{Acceptor}$ is the concentration of the drug in the acceptor compartment at the end of the assay. $[Drug]_{Equilibrium}$ is determined by measuring the concentration of a reference solution, containing the drug at the theoretical equilibrium concentration (the overall concentration of the donor and acceptor solutions combined). Given that the acceptor and donor compartments used in this study had a volume of 300 µL and 150 µL respectively, the equilibrium concentration of the drug should theoretically be one-third of that of the original solution added to the donor well.

### 2.9. High-Performance Liquid Chromatography (HPLC)

HPLC was carried out at RT with a Shimadzu 10Avp HPLC system (Kyoto, Japan). A Luna C18 (2) column was used, with a length of 250 mm, internal diameter of 4.6 mm and 5 µm particle size. The mobile phase consisted of 13 volumes of acetonitrile and 87 volumes of a 2.45 g/L solution of phosphoric acid, previously adjusted to pH 3.0 with triethylamine. An injection volume of 10 µL and flow rate of 1.5 mL/min for 15 min was used. A Shimadzu SPD-10Avp UV-vis detector at 278 nm was used to detect the drug. The calibration curve used was linear over the CIP concentration range of 0.0025–0.02 mg/mL ($R^2$=0.9999) with limit of detection (LOD) and limit of quantification (LOQ) values of 0.17 and 0.57 µg/mL, respectively. The percent relative standard deviation (%RSD) was 0.66%.

### 2.10. Statistical Analysis

Statistical analysis was carried out using Minitab® 16 software. Data was analyzed using one-way analysis of variance (ANOVA) with Tukey's multiple comparison test and two-sample Student *t* tests. A *p*-value of $\leq 0.05$ was considered significant.

## 3. Results and Discussion

### 3.1. Ball Milling of Pure Amino Acids

Ball milling was first carried out on the amino acids themselves. This proved ineffective at amorphizing the amino acids, with only slight decreases in the intensity of their PXRD patterns noted after 4 hours of milling (Fig. 3). Similarly, when CIP was ball milled on its own it became more disordered, but remained partially crystalline [2]. Löbmann et al were also unable to produce amorphous amino acids via ball milling [8]. Like CIP, amino acids have high melting points and strong crystal lattices, making them difficult to amorphize on their own [10]. They are also relatively small and simple molecules, and can therefore recrystallize quickly [21]. In addition to ball milling, spray drying, vacuum drying and cryomilling have all proven unsuccessful at amorphizing amino acids, while quench cooling results in their degradation [8,9,11]. Pure amorphous ARG has been generated via freeze drying, however this production method was unsuccessful for other amino acids [9].

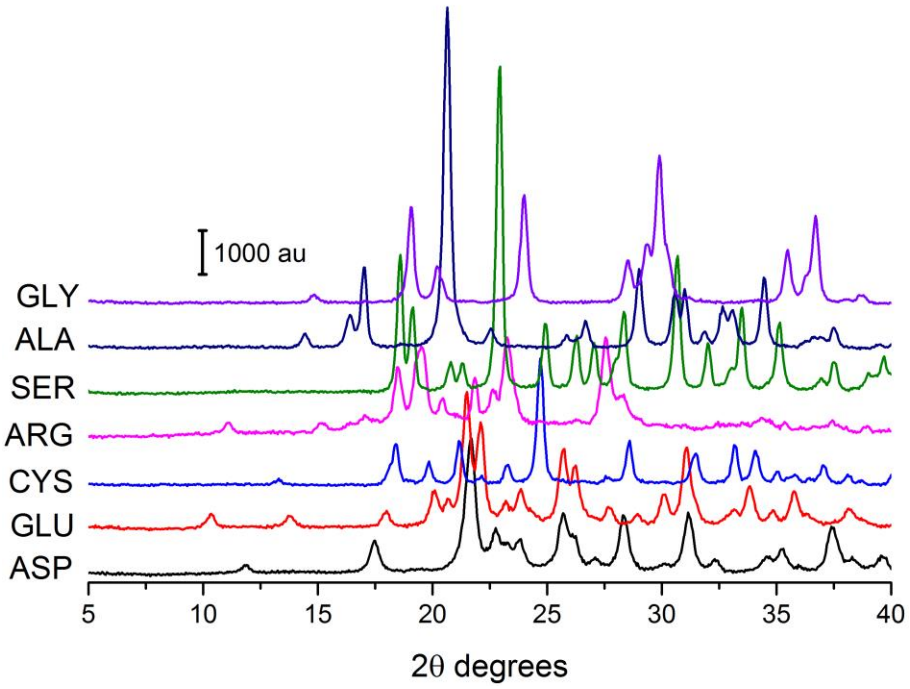


**Fig. 3.** PXRD analysis of ball milled amino acids.

### 3.2. Production of Ciprofloxacin/Amino Acid Solid Dispersions

Similar to CIP, the α-carboxylate and amino groups, as well as the side chains of relevant amino acids, are involved in a number of intermolecular hydrogen bonds in the crystal lattice of these compounds. The formation of CIP/amino acid salts should therefore facilitate amorphization of both moieties, by disrupting this bonding network and preventing nucleation during processing [22]. This was attempted by ball milling CIP with the seven amino acids mentioned above in a 1:1 molar ratio. This ratio has been used for most amorphous drug-amino acid formulations described in the literature to date, and has been shown to result in the most stable ball milled formulations [23].

Following the successful production of CIP aspartate and glutamate salts reported by Elshaer et al [14], it was predicted that CIP would also form amorphous formulations with these amino acids via ball milling. After four hours of milling, a few small peaks remained in the PXRD diffractograms of CIP/ASP and CIP/GLU. However, when milled for a further two hours they became fully X-ray amorphous (Fig. 4). Surprisingly, when CIP was milled with CYS and ARG, fully X-ray amorphous formulations were obtained after only four hours of milling (Fig. 4). This was particularly unexpected for ARG, as Elshaer et al were unable to produce CIP salts with any of the basic amino acids [14]. Similarly, when the twenty essential amino acids were screened by Kasten et al for their suitability as amorphous co-formers for several drugs, it was discovered that ARG could only amorphize acidic compounds. In addition, the authors concluded that ASP and GLU were poor stabilizers for all drugs included in their study, while CYS was only successful for the acidic drug furosemide. The amino acids SER, ALA and GLY were also unsuccessful co-formers for all of the drugs included in Kasten et al's study [24]. Likewise, when CIP was milled with these amino acids for four hours, semi-crystalline solid dispersions were obtained, with PXRD patterns matching the most intense peaks of the starting materials. For the ease of discussion, these amorphous and semi-crystalline CIP/amino acid formulations will henceforth be referred to as amorphous solid dispersions (ASDs) and solid dispersions (SDs), respectively.

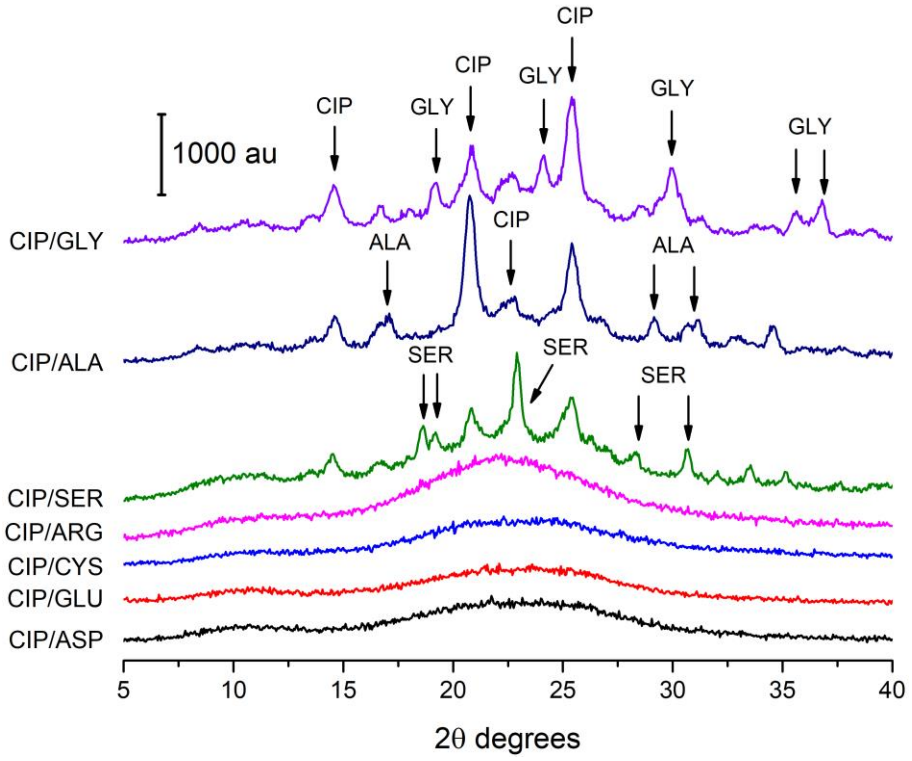


**Fig. 4.** PXRD analysis of ball milled CIP/amino acid ASDs and SDs. CIP/ASP and CIP/GLU were milled for a total of 6 hours, while the remaining samples were milled for 4 hours. The arrows point to the location of the most prominent peaks of CIP, SER, ALA and GLY.

There are a number of possible explanations as to why some amino acids formed ASDs with CIP, while others did not. It is possible that the size of the amino acids had an influence on their ability to interact with CIP. It could be hypothesized that the smaller size of GLY, ALA and SER would facilitate their interaction with the drug. However, these simple amino acids all resulted in partially crystalline SDs when ball milled with CIP. On the other hand, the bulkier side chains and higher molecular weight of ASP, GLU, CYS and ARG may have increased the configurational entropy of the ASDs containing these amino acids, and thus hindered their crystallization [21].

The reason why only some of the amino acids were successful co-formers for the amorphization of CIP may be due to $pK_a$ differences. The $pK_a$ values of CIP have been reported as 6.16 and 8.62 for the carboxylic acid and piperazine secondary amine, respectively [25]. The $pK_a$ values of the α-carboxylic acid groups, α-amino groups and relevant side chains of the amino acids have been reported by Berg et al, and are listed in Table 1 [26]. In a previous study, the piperazine amino group of CIP was found to interact with the carboxylate groups of polymers, resulting in the formation of polymeric salts [3], and a similar interaction is believed to occur in the amino acid ASDs studied here (see next section). From Table 1 it can be seen that the amino acids with the lowest α-COOH $pK_a$ values (thereby providing the greatest difference in $pK_a$ from that of the piperazine amino group of CIP) are ARG and CYS. These amino acids formed ASDs most readily with the drug, requiring only four hours of milling. ASP and GLU have slightly higher $pK_a$ values for their α-COOH groups, and required a further two hours of milling with CIP to become fully X-ray amorphous. Due to their higher $pK_a$ values, the side chain carboxylic acid groups of ASP and GLU are less likely to form an ionic interaction with CIP than their α-carboxylate groups. Although the equivalent $pK_a$ difference of SER is on par with than that of ASP and GLU, it was unable to form an ASD with CIP via ball milling. This suggests that a combination of factors influences the successful co-amorphization of CIP with an amino acid, including the $pK_a$ of the α-carboxylic acid group and its molecular weight.

**Table 1**. $pK_a$ Values of CIP and the Amino Acids Used in this Study

| **Amino Acid** | **COOH** | **$NH_2$** | **Side chain** | **$\Delta pK_a$[a]** |
|---|---|---|---|---|
| CIP | 6.2 | 8.6 | N/A | N/A |
| ASP | 2.0 | 10.0 | 3.9 | 6.6 |
| GLU | 2.2 | 9.7 | 4.3 | 6.4 |

| | | | | |
|---|---|---|---|---|
| CYS | 1.8 | 10.8 | 8.3 | 6.8 |
| ARG | 1.8 | 9.0 | 12.5 | 6.8 |
| SER | 2.1 | 9.2 | N/A | 6.5 |
| ALA | 2.3 | 9.9 | N/A | 6.3 |
| GLY | 2.4 | 9.8 | N/A | 6.2 |

[a]$\Delta pK_a$: Difference in $pK_a$ between the piperazine amino group of CIP and the α-COOH groups of the amino acids.

### 3.3. Analysis of Drug-Amino Acid Interactions

#### 3.3.1. Fourier Transform Infrared Spectroscopy

The FTIR spectra of crystalline CIP, the amino acids, ASDs and PMs are shown in Fig. 5. The FTIR spectrum of CIP contains a number of peaks that are characteristic of the zwitterionic form of the drug. The peaks at 1590 $cm^{-1}$ and 1375 $cm^{-1}$ correspond to the asymmetric and symmetric stretching vibrations, respectively, of the carboxylate ion of CIP [27]. These peaks were also present in the spectra of the SDs containing SER, ALA and GLY, but absent from those of the CIP/amino acid ASDs. In contrast, the spectra of all of the ASDs contain a peak at 1720–1725 $cm^{-1}$, which may be attributed to the carbonyl stretch of the unionized carboxylic acid group of CIP (Fig.5b) [2,3]. In the case of CIP/ARG this peak appears as a broad shoulder due to significant overlap with the neighboring guanidyl peak. The ketone carbonyl stretch of CIP ($C_7$=O) underwent a shift from 1618 $cm^{-1}$ to 1627–1628 $cm^{-1}$ in the spectra of the amino acid ASDs, which provides further evidence that the carboxylic acid group of CIP is unionized [2,3]. The partial conversion of the carboxylate group of CIP to the protonated form in the three semi-crystalline SDs was confirmed by the presence of a small peak at 1720–1725 $cm^{-1}$ in their FTIR

spectra (Fig. 5c). In addition, the ketone carbonyl stretches of the CIP/SER and CIP/ALA SDs were shifted to 1627 $cm^{-1}$ and 1623 $cm^{-1}$, respectively, whereas no such shift was detected with CIP/GLY.

$NH_2^+$ stretching vibrations are present as weak bands at 2400–2600 $cm^{-1}$ in the FTIR spectrum of CIP [6], and small bands may also be seen in this region in the spectra of all of the ASDs and semi-crystalline SDs. Therefore, it appears that CIP is in the same ionization state in these amorphous formulations as in the CIP salts and CIP/polymer ASDs that are described in the literature, i.e. with an unionized carboxylic acid group and a protonated secondary amine [3,6]. This latter group most likely interacts with the α-carboxylate groups of the amino acids, thereby forming salts. While a portion of CIP also underwent proton transfer when milled with SER, ALA and GLY, the drug-amino acid interactions were apparently not of sufficient strength to amorphize these samples completely.

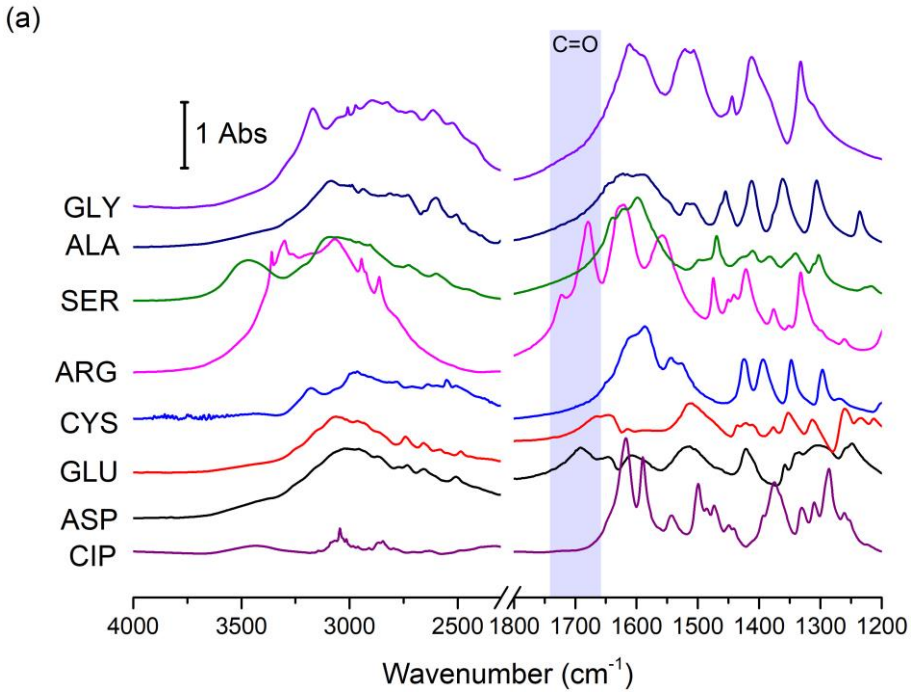
(a)
C=O
1 Abs
GLY
ALA
SER
ARG
CYS
GLU
ASP
CIP
4000
3500
3000
2500
1800
1700
1600
1500
1400
1300
1200
Wavenumber (cm-1)

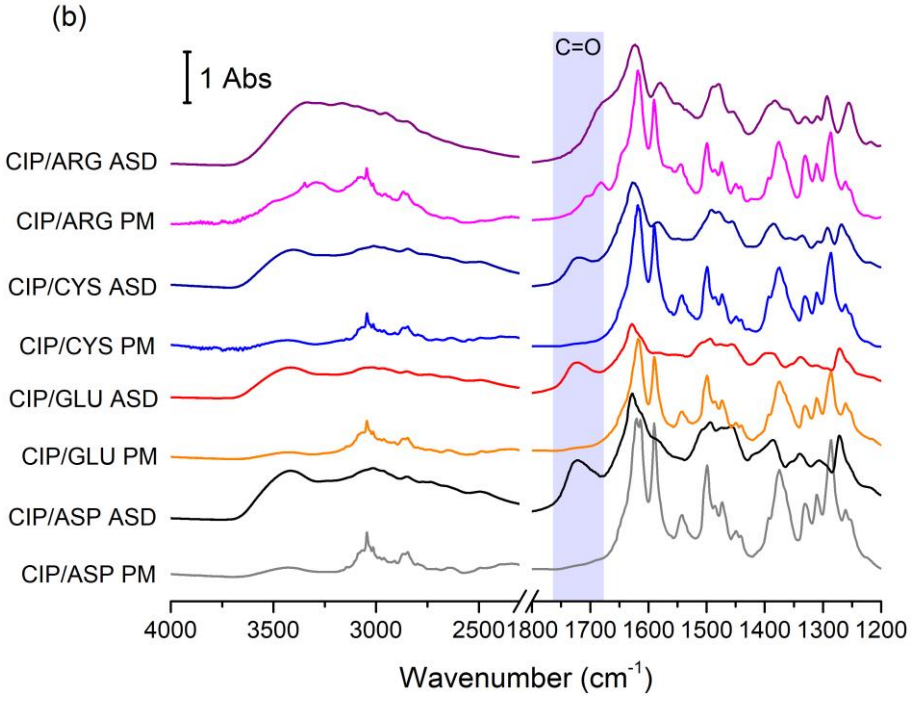
(b)
C=O
1 Abs
CIP/ARG ASD
CIP/ARG PM
CIP/CYS ASD
CIP/CYS PM
CIP/GLU ASD
CIP/GLU PM
CIP/ASP ASD
CIP/ASP PM
4000
3500
3000
2500
1800
1700
1600
1500
1400
1300
1200
Wavenumber (cm-1)

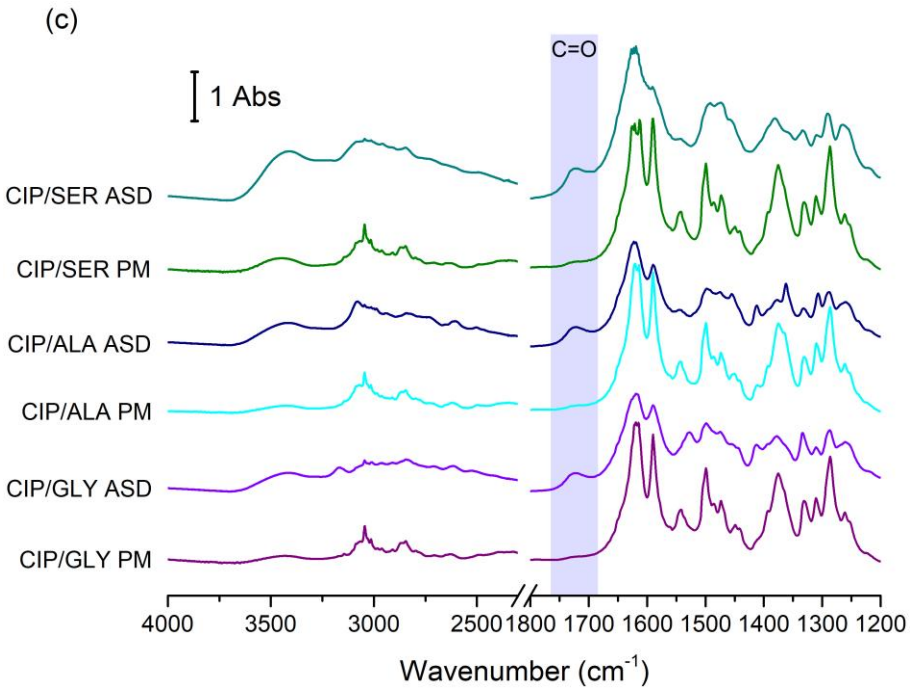


**Fig. 5.** FTIR spectra of (a) starting materials (b) ASDs and corresponding PMs and (c) semi-crystalline SDs and corresponding PMs. Peaks corresponding to the C=O stretch of carboxylic acid groups are highlighted in violet.

### 3.3.2. Solid-State Nuclear Magnetic Resonance

The $^{13}C$ CP/MAS NMR spectra of crystalline CIP, the ball milled amino acids, and the ASDs and corresponding PMs are shown in Fig. 6. As the side chains of the acidic amino acids differ by only one $CH_2$ group, SSNMR was not carried out on the samples containing ASP.

The $^{13}C$ spectrum of crystalline CIP matches that obtained by Mafra et al for the zwitterionic form of the drug [28]. Full peak assignment has been carried out by this group, and this was used to identify the peaks in the spectra of the CIP/amino acid ASDs. The $^{13}C$ spectra of the ball milled pure amino acids match those of crystalline GLU [29], CYS [30] and ARG [31], which have previously been described. The peaks present in these spectra are sharp in appearance,

confirming that ball milling did not alter the crystallinity, ionization state or intermolecular interactions of the amino acids. Similarly, no significant differences were seen in their FTIR spectra following ball milling (data not shown). In contrast, the $^{13}C$ NMR spectra of the ASDs contain broad and overlapped peaks, which is typical of disordered solids and confirms their amorphous nature [32]. The spectra of the PMs consist of a direct combination of those of crystalline CIP and the ball milled amino acids, and no changes in peak chemical shift were detected.

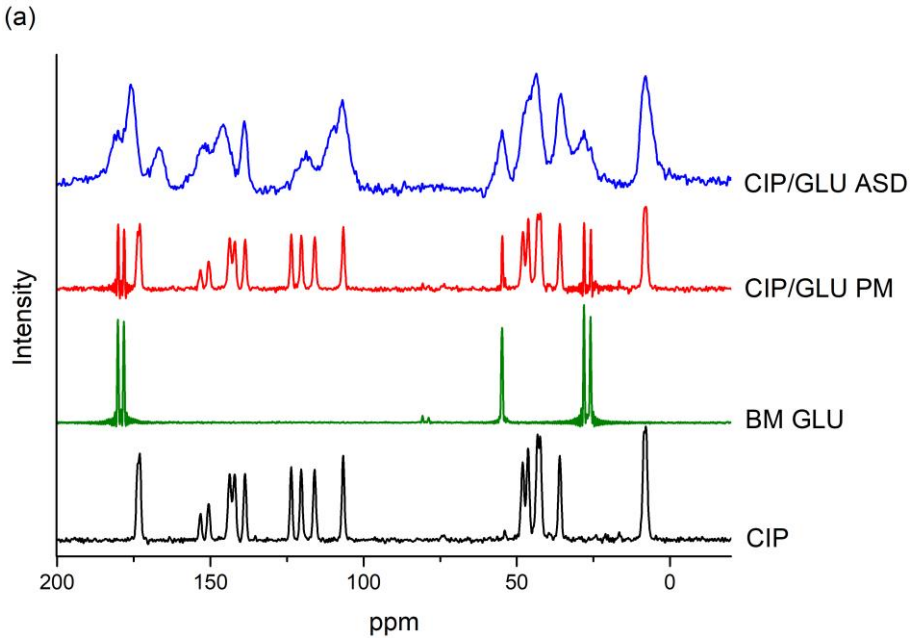

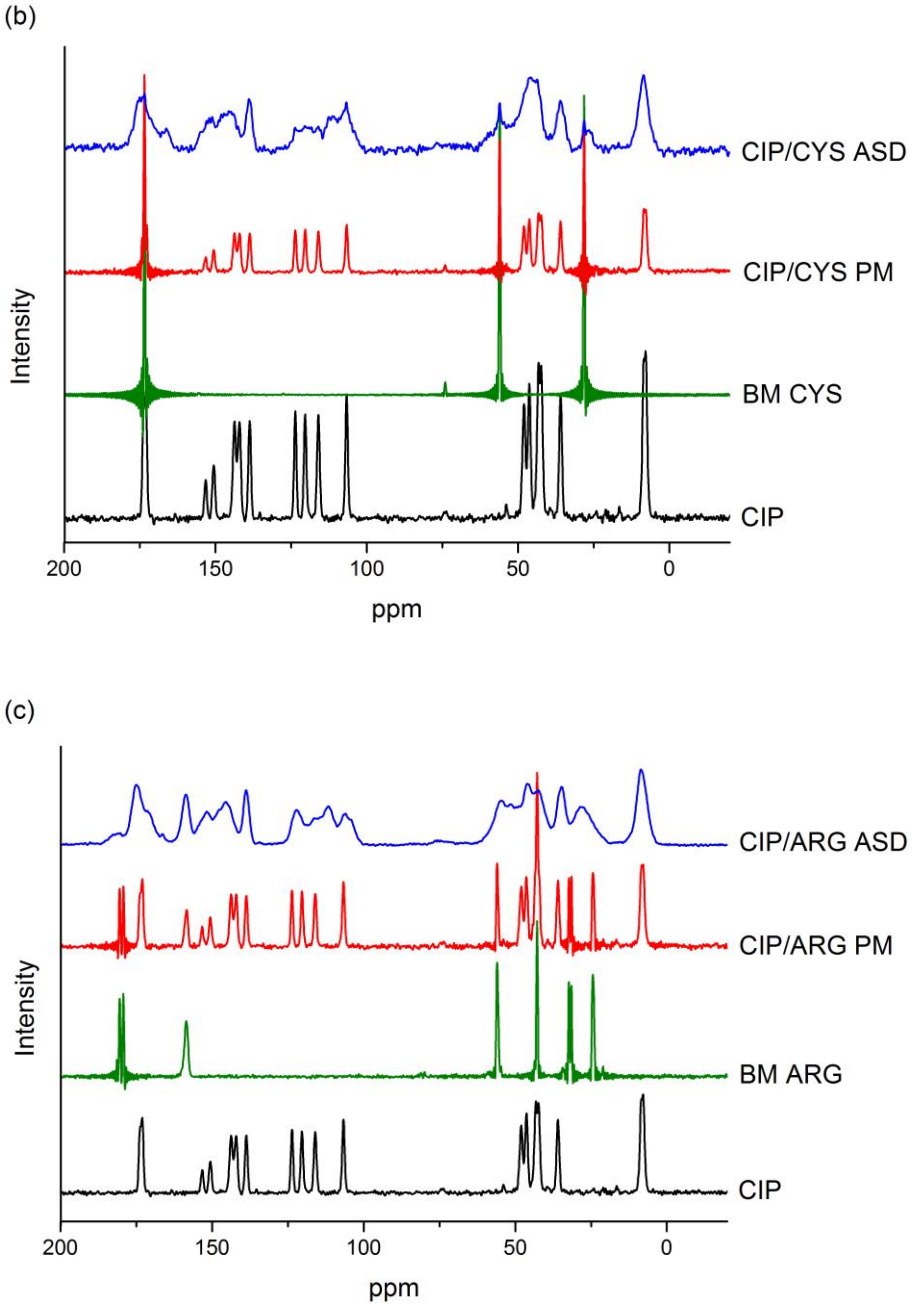


**Fig. 6.** $^{13}$C CP/MAS NMR spectra of samples containing (a) GLU (b) CYS and (c) ARG. BM: ball milled.

Of particular interest in this study was the location of the peaks corresponding to the carbonyl groups of CIP. If our hypothesis concerning the ionization state of CIP in the ASDs is correct,

these peaks should undergo certain shifts due to protonation of the carboxylate group of the drug. Therefore, the carbonyl region of the spectra (~160–190 ppm) will be focused on here. The relevant peak shifts for the samples are listed in Table 2.

**Table 2.** SSNMR $^{1}H$ $T_1$ Spin-Lattice Relaxation Times and Carbonyl Peak Assignment

| Sample | $^{1}H$ $T_1$ (s) | Chemical Shift (ppm) | Assignment |
|---|---|---|---|
| CIP | 12 | 173.0 | $C_6$=$OO^-$ |
| | | 173.7 | $C_7$=O |
| BM[a] GLU | 7.2 | 178.2 | $C_{SC}$=OOH[b] |
| | | 180.2 | $C_\alpha$=$OO^-$ |
| BM CYS | 3.3 | 173.5 | $C_\alpha$=$OO^-$ |
| BM ARG | 13.5 | 179.4 | $C_\alpha$=OOH |
| | | 180.6 | $C_\alpha$=$OO^-$ |
| CIP/GLU ASD | 2.0 | 166.7 | $C_6$=OOH |
| | | 175.5 | $C_7$=O |
| | | 178.2 | $C_{SC}$=OOH |
| | | 180.2 & 181.2 | $C_\alpha$=$OO^-$ |
| CIP/CYS ASD | 1.9 | 166.2 | $C_6$=OOH |
| | | 173.5 | $C_\alpha$=$OO^-$ |
| | | 175.4 | $C_7$=O |
| CIP/ARG ASD | 1.2 | 166.4 | $C_6$=OOH |
| | | 175.1 | $C_7$=O |
| | | 180.7 | $C_\alpha$=$OO^-$ |

[a]BM: ball milled. [b]$C_{SC}$=OOH: side chain carboxylic acid.

The peak corresponding to the carboxylate carbonyl carbon of zwitterionic CIP ($C_6$ according to the numbering system in Fig. 1) appears at 173.0 ppm [28]. In the spectra of the ASDs this peak is shifted to 166.2–166.7 ppm. In the zwitterion, $C_6$ is part of an electronegative carboxylate

group, resulting in greater deshielding than in the unionized form of the drug, and a higher chemical shift. A similar shift was seen with the equivalent peak in the $^{13}C$ spectrum of sparfloxacin. The carboxylate carbonyl peak of zwitterionic sparfloxacin trihydrate appears at 169 ppm, whereas that of the unionized form of the drug is located at 164.5 ppm [33]. The $^{13}C$ SSNMR spectrum of the CIP saccharinate salt, in which the carboxylic acid of CIP is unionized, was also found to contain a peak at 166.5 ppm, whereas this peak was absent from the spectra of the raw materials [34].

In contrast to the carboxylic acid carbonyl of CIP, the ketone carbonyl, which appears at 173.7 ppm in the spectrum of the crystalline drug, is shifted slightly downfield in the ASDs, to 175.1–175.5 ppm (Table 2). Similarly, the equivalent carbonyl group demonstrated a higher chemical shift in the $^{13}C$ NMR spectrum of unionized sparfloxacin compared to the zwitterion [33]. As discussed in the previous section, the peak corresponding to the $C_7$ carbonyl stretch also shifted to higher wavenumbers in the FTIR spectra of the ASDs, and this may be attributed to changes in the hydrogen bonding of this group. When the carboxylic acid of CIP is protonated, an intramolecular hydrogen bond forms between this group and the neighboring ketone group, resulting in the formation of a constrained six-membered ring [2], which appears to have a deshielding effect on the ketone carbon. The results of the SSNMR studies therefore reinforce the hypothesis that the carboxylic acid of CIP is unionized in these ASDs, and it can be concluded that proton transfer to the carboxylate group of the drug occurred during the milling process. This is unlikely to be due to the conversion of zwitterionic CIP to the unionized form, as ball milling has been proven to be ineffective at bringing about this transformation [2]. Therefore, the piperazine amino group of CIP is most likely ionized in the ASDs, as suggested by the results of FTIR analysis. The interaction of this positively charged group with the anionic

α-carboxylate groups of the amino acids would result in proton transfer from the amino acid to the drug, and the formation of a salt. No significant changes in the chemical shifts of the carbonyl groups of the amino acids were seen in the $^{13}C$ NMR spectra of the ASDs compared to the pure ball milled amino acids, and therefore their α-carboxylate groups appear to remain ionized in the ASDs. As previously mentioned, CIP is more likely to form ionic bonds with the α-carboxylate groups of ASP and GLU rather than the side chain carboxylic acids due to their lower $pK_a$ values.

Another indicator that proton transfer occurs from the amino acids to CIP upon milling is that the four ASDs were an intense yellow color, whereas the starting materials are white or off-white. A similar change in color was also observed with the amorphous CIP/succinic acid salts and polymeric salts described previously [3,6]. This supports the assumption that CIP is forming a salt with the amino acids in these ASDs. In contrast, the semi-crystalline SDs were pale yellow following milling, due to the small degree of proton transfer that occurred in these samples.

Unlike the other amino acids, the crystalline ARG starting material used in this study appears to be a mixture of the unionized and zwitterionic form of the amino acid, as its PXRD pattern (Fig. A.1a, Supplementary Material) matches that reported by Patel et al. The authors claimed that the crystalline ARG used in their study was a mixture of phases, consisting of the zwitterionic dihydrate plus unionized ARG [13]. This would explain the presence of two peaks in the carbonyl region of ARG's $^{13}C$ NMR spectrum (Fig. 6c and Table 2). The peak corresponding to the α-carboxylate carbonyl of ARG appears upfield when it is protonated, due to the increased shielding effect of the unionized carboxylic acid group [13]. Therefore, the peaks at 180.6 ppm and 179.4 ppm in the $^{13}C$ spectrum of ball milled ARG may be attributed to the zwitterionic and unionized form of the amino acid, respectively.

In addition to the determination of intermolecular interactions, SSNMR can also provide information on the mobility and miscibility of an ASD, via measurement of the spin-lattice relaxation time ($^1$H $T_1$). The $^1$H $T_1$ of a solid decreases upon amorphization due to an increase in molecular mobility, which enables energy transfer [32]. The $^1$H $T_1$ values of all of the ASDs were significantly lower than those of crystalline CIP and the amino acids, which confirms their amorphous nature (Table 2). If the two components of a mixture are molecularly mixed they will have a common $T_1$ [32]. This was the case with the CIP/amino acid ASDs, which suggests that they consist of a single amorphous salt phase.

### 3.4. Thermal Analysis

The DSC thermograms of the amino acid ASDs and SDs obtained with a heating rate of 10 $^{o}$C/min are shown in Fig. 7, and a summary of their thermal properties is given in Table 3. DSC thermograms of the amino acid starting materials and CIP/amino acid PMs are shown in Fig. A.2 (Supplementary Material).

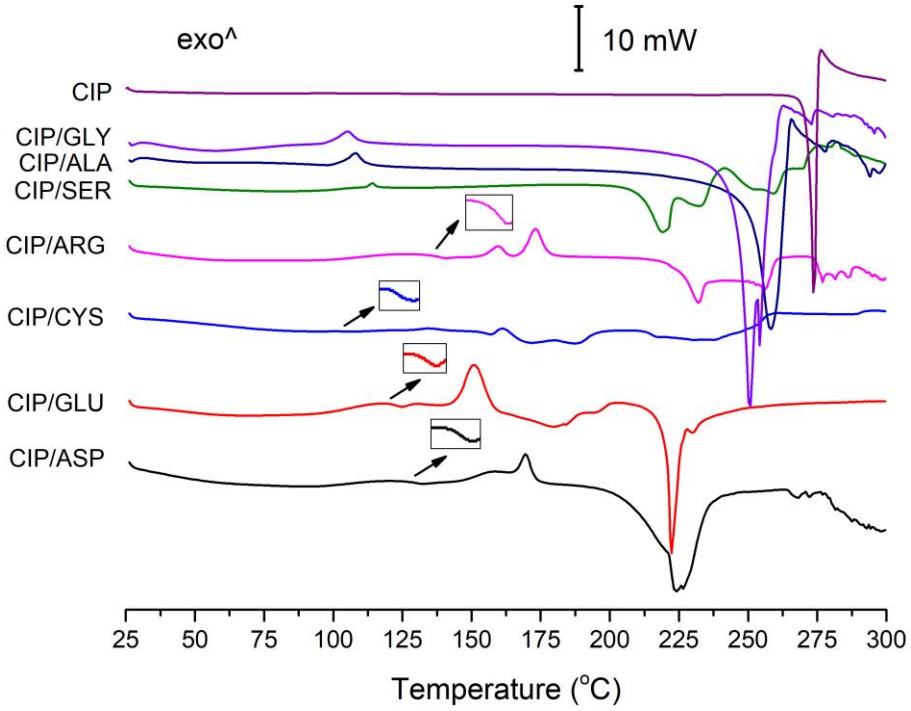


**Fig. 7.** DSC thermograms of crystalline CIP starting material and CIP/amino acid ASDs and SDs. The enlarged glass transitions of the ASDs are shown in the insets.

**Table 3.** Thermal Properties of CIP/Amino Acid ASDs and SDs Heated at 10 °C/min[a]

| Sample | $T_g$ (°C) | Crystallization onset (°C) | Crystallization peak (°C) |
|---|---|---|---|
| CIP/ASP | 135.8 ± 0.6 | 168.4 ± 0.5 | 171.3 ± 0.3 |
| CIP/GLU | 121.7 ± 0.9 | 149.2 ± 0.3 | 154.5 ± 0.1 |
| CIP/CYS | 104.0 ± 0.1 | 157.8 ± 0.0 | 161.1 ± 0.1 |
| CIP/ARG | 136.9 ± 0.5 | 153.7 ± 0.7/ 166.4 ± 1.7 | 158.8 ± 0.9/ 169.7 ± 0.2 |
| CIP/SER | N.D. | 111.3 ± 0.6 | 113.8 ± 0.5 |
| CIP/ALA | N.D. | 102.8 ± 0.2 | 108.1 ± 0.2 |
| CIP/GLY | N.D. | 98.2 ± 0.8 | 104.3 ± 0.8 |

[a]The average of three measurements is shown, ± the standard deviation.

### 3.4.1. Glass Transition

With each of the ASDs, a $T_g$ was detected above that of pure amorphous spray dried CIP (equal to 86.7 $^oC$) [2]. Due to the inherent difficulty in producing amorphous amino acids, there is little information in the literature concerning the glass transition of pure amino acids. However, the $T_g$ of freeze dried amorphous ARG has been independently reported as 55 $^oC$ [35] and 18.4 $^oC$ [10], while the $T_g$'s of freeze dried solutions containing 5% gelatin plus 10% ALA or SER in water were found to be -21.55 and -18.75 $^oC$, respectively [36]. The $T_g$'s of freeze dried GLY and GLU have also been reported as approximately 7 $^oC$ [37] and -17 $^oC$ [38], respectively. Unfortunately, the $T_g$'s of ASP and CYS could not be found in the literature. However, based on the published $T_g$ values of other amino acids, it is reasonable to assume that they are significantly lower than those of the ASDs. Therefore, the measured $T_g$'s of the CIP/amino acid ASDs are much higher than what would be expected if the two components were simply mixed intimately together. This provides further evidence of amorphous salt formation.

Due to their low amorphous content, a $T_g$ could not be detected for the three semi-crystalline SDs. High-speed DSC (HSDSC) was therefore carried out on the samples. When a higher heating rate is used for DSC, the same heat flow will occur over a shorter length of time. This causes signals to become larger, enabling low-energy transitions to be detected and measured [39]. As the heating rate was increased, the glass transitions of the ASDs appeared as larger step changes in the thermograms (Fig. A.3, Supplementary Material). However, despite the use of heating rates of up to 300 $^oC$/min, the $T_g$'s of the SDs could not be detected.

### 3.4.2. Crystallization

All of the ASDs underwent cold crystallization during DSC analysis, with onset temperatures approximately 30 $^oC$ above the $T_g$. Small crystallization peaks could also be seen in the

thermograms of the semi-crystalline SDs, confirming that a small portion of material was transformed to the amorphous phase. The onset of crystallization occurred at much higher temperatures with the ASDs than the SDs, indicating that they possess superior physical stability [11].

In order to determine the species that crystallized from the ASDs and SDs during DSC analysis, PXRD and FTIR were carried out on all of the samples immediately following the endset of crystallization. In the case of the semi-crystalline SDs containing GLY, ALA and SER, the PXRD patterns matched those obtained after ball milling, i.e. with low intensity peaks matching those of zwitterionic CIP and the amino acid starting materials (Fig. A.4a, Supplementary Material). The PXRD pattern of CIP/SER contained an additional peak at 9.2 2θ degrees, which corresponds to the unionized form of CIP. Despite the fact that CYS appears to form a salt with CIP following four hours of ball milling, the ASD containing this amino acid also crystallized to zwitterionic CIP during DSC analysis. This suggests that the interactions between the drug and CYS were not of a sufficient strength to maintain the salt structure upon heating.

The DSC thermogram of the CIP/ARG ASD differs from the other samples by the presence of two exotherms. If crystal nuclei remain following ball milling, an initial exotherm will appear during DSC analysis due to surface crystallization, while a second peak will develop due to bulk crystallization [40]. In order to determine whether these peaks correspond to a two stage crystallization process, or to the formation of an intermediate phase, CIP/ARG was analyzed by PXRD immediately after each crystallization event. The diffraction patterns obtained in both instances were almost identical, but grew in intensity following the second crystallization exotherm. Therefore, it can be concluded that the formation of an intermediate phase did not occur [40]. Instead, the appearance of two exothermic peaks suggests that the CIP/ARG particles

may have contained a number of surface crystal nuclei following milling, which were too small to be detected by PXRD [40]. A second small, broad exotherm was also visible in the thermogram of CIP/CYS, with a peak at approximately 180 $^{o}$C. The PXRD pattern obtained following this transition was identical to that obtained after the primary crystallization exotherm (i.e. matching that of zwitterionic CIP), however there was a slight increase in peak intensity, due to further crystallization of the sample. The use of high heating rates can reduce the likelihood of amorphous solids crystallizing during DSC analysis. However, crystallization peaks were still present in the thermograms of all of the CIP/amino acid ASDs when heated at rates of up to 300 $^{o}$C/min (Fig. A.3, Supplementary Material), indicating that the molecules have high mobility [41]. A double exotherm was also observed with the CIP/ARG ASD at all heating rates, which indicates that the surface of this sample crystallizes very quickly [21].

In contrast to the other samples, the major phase identified following the crystallization of CIP/ARG was that of the unionized form of CIP, while a peak of ARG was also present at approximately 19.6 2θ degrees (Fig. A.4a, Supplementary Material). The FTIR spectrum of this sample also matched that of the unionized form of CIP [2], with a peak at 1729 cm$^{-1}$ due to the presence of the protonated carboxylic acid of the drug (Fig. A4b, Supplementary Material). Therefore, like CIP/CYS, the arginine salt dissociated upon heating.

Unlike the other CIP/amino acid formulations, the PXRD patterns of the solids collected after crystallization of the CIP/ASP and CIP/GLU ASDs did not entirely match those of the starting materials. However, their FTIR spectra were very similar to those obtained with the freshly milled ASDs, although there were differences in peak intensity (Fig. A.4b, Supplementary Material). This indicates that CIP, ASP and GLU are in the same ionization state following crystallization, and that their ionic hetermolecular interactions remain intact. It was therefore

hypothesized that the unidentified PXRD peaks belong to crystalline CIP aspartate and CIP glutamate salts. In order to verify this, attempts were made to produce these salts. However, this proved very difficult due to the poor solubility of CIP in water and other common solvents. In most cases pure CIP hydrate, aspartic acid or glutamic acid crystallized. Only slow crystallization of a 1:2 molar solution of CIP and amino acid in a water/ethanol mixture resulted in a solid with PXRD peaks resembling those obtained following DSC crystallization of these ASDs (Fig. 8). Unfortunately, it was not possible to obtain pure crystals of a sufficient quality for single crystal X-ray analysis, and therefore the chemical composition of these samples could not be ascertained.

For comparison, a portion of the CIP/ASP and CIP/GLU ASDs were left exposed at RT to enable their slow crystallization. In the case of CIP/ASP, the crystals produced by slow solvent evaporation and RT crystallization of the ASD had very similar PXRD patterns (Fig. 8). Additional peaks were present at 21.7, 22.9 and 23.8 2θ degrees in the diffractogram of the former sample due to contamination with residual crystalline ASP. The peak at 5.1 2θ degrees in the diffractogram of this sample does not correlate with any of the raw materials, and may be due to the formation of a new phase, such as a hydrate of CIP aspartate. The PXRD diffractogram of the CIP/ASP ASD that crystallized during DSC analysis contained distinctive peaks at approximately 9.3, 9.9, 26.0 and 27.3 2θ degrees, and these were also present in the diffractograms of the other CIP/ASP crystals. Additional peaks in the diffractogram of the solid obtained following DSC crystallization match those of anhydrous zwitterionic CIP. Therefore this sample crystallizes to a mixture of phases during DSC analysis.

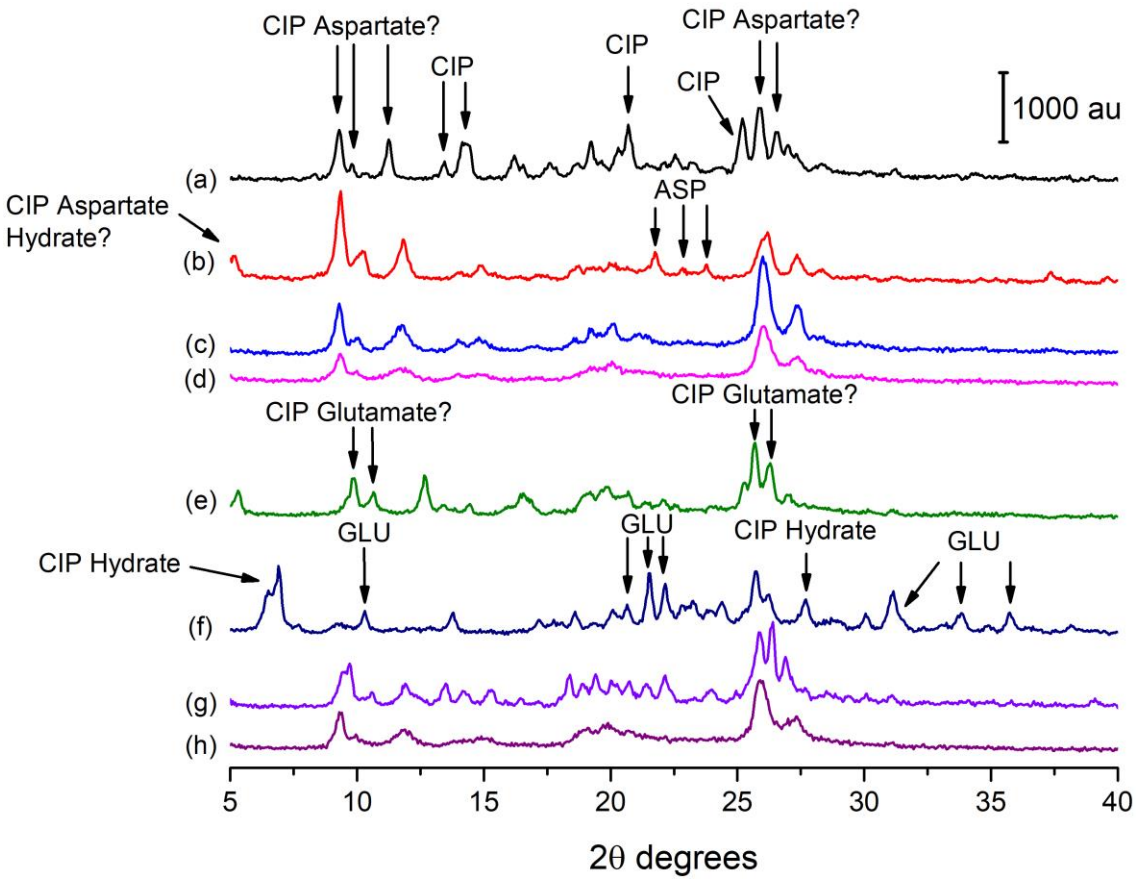


**Fig. 8**. PXRD analysis of CIP/ASP and CIP/GLU crystals: (a) CIP/ASP ASD post DSC crystallization (b) CIP/ASP post slow evaporation from ethanol/water (c) CIP/ASP ASD post RT crystallization x 2.5 months (d) CIP/ASP ASD post RT crystallization x 1 week (e) CIP/GLU ASD post DSC crystallization (f) CIP/GLU post slow evaporation from ethanol/water (g) CIP/GLU ASD post RT crystallization x 2.5 months (h) CIP/GLU ASD post RT crystallization x 1 week. The arrows identify the principal peaks of the phases.

Solvent evaporation of a solution of CIP and GLU was unsuccessful at producing the CIP glutamate salt, and instead resulted in the crystallization of CIP 3.7 hydrate [28] and GLU starting material. In contrast, when the CIP/GLU ASD was left exposed at RT for one week, its PXRD pattern did not correspond to any of the starting materials. However, it was almost

identical to that of the CIP/ASP ASD that was crystallized in the same manner (Fig. 8). If we are correct in our assumption that the CIP aspartate and glutamate salts are crystallizing from the corresponding ASDs, then the similarity of the PXRD patterns of these salts suggests that they are isostructural, i.e. they have a similar molecular packing but different chemical composition. Similarly, the PXRD patterns of a number of lamotrigine salts were found to closely resemble each other, and this was attributed to their isostructural nature. Although they were formed using different solvents and contained various dicarboxylic acids as counterions, the salts had the same packing arrangements and hydrogen bonding motifs [42].

Following 2.5 months of exposure at RT, the peaks present in the diffractogram of the CIP/GLU ASD became more distinct, and a number of additional peaks appeared. Matching peaks were identified at approximately 9.8, 10.6, 21.4, 22.1, 25.8 and 26.3 2θ degrees in the diffractograms of the ASDs crystallized at RT and during DSC analysis. The latter sample also contained a number of additional peaks, which did not correspond to any of the raw materials. Therefore, this ASD also seems to crystallize to a mixture of phases during DSC analysis, possibly consisting of the CIP glutamate salt, plus an unidentified phase or phases.

### 3.4.3. Melting

All of the ASDs and SDs undergo melting accompanied by decomposition at temperatures above 200 $^{o}$C, which is not surprising given the high melting point of crystalline CIP and the amino acids (Fig. A.2a, Supplementary Material). The drug and the amino acid starting materials also appear to undergo significant decomposition upon melting, resulting in broad melting endotherms and complex thermograms. TGA was used to quantify this thermal degradation (Fig. A.5, Supplementary Material). An initial decrease in mass occurred from 25–100 $^{o}$C with the

four ASDs, due to the loss of sorbed water. This is to be expected for amorphous formulations due to their hygroscopic nature. A substantial total loss in mass of 20–34% was obtained with the ASDs, and they began to degrade at lower temperatures than the corresponding PMs. This may be due to the higher molecular mobility of the amorphous samples, which can increase their reactivity and thus make them more prone to chemical degradation [32].

The higher heating rates used in HSDSC should reduce the degree of degradation of a sample, as there will simply be less time for this to occur [43]. Although the thermograms of the ASDs and SDs were smoother when heated at 300 ºC/min, substantial degradation still occurred with each sample upon melting, as can be seen from the complexity of the thermograms above 200–250 ºC (Fig. A.3, Supplementary Material**)**.

### 3.5. Stability Studies

The DVS isotherms of the CIP/amino acid ASDs are shown in Fig. 9. Like many amorphous solids, these samples have a great propensity for water sorption. The large free volume and irregular molecular arrangement of amorphous materials allows for water uptake into the bulk of the material rather than just surface adsorption [44]. The greatest increase in mass during DVS analysis was obtained with CIP/ASP, reaching 31.0% at 90% RH, followed by CIP/ARG (23.9%), CIP/CYS (21.1%) and CIP/GLU (17.9%).

Unlike the other ASDs, the isotherm of CIP/ASP is concave in shape and shows minimal hysteresis. This suggests that water is mainly adsorbed to the surface of particles in this sample, and does not enter the interior significantly. In contrast, considerable hysteresis was observed

with the other ASDs. Hysteresis is commonly encountered with amorphous solids due to water absorption into the bulk of the particles [45]. Therefore, the water uptake mechanism of the ASDs containing GLU, CYS and ARG differs from that of CIP/ASP, which may be due to differences in porosity.

Hysteresis was particularly evident in the isotherm of the CIP/ARG ASD, as the sample mass did not return to its original value at the end of the desorption cycle. Hysteresis may occur due to the failure of a sample to equilibrate fully during DVS analysis, i.e. if too short an equilibration time is used [46]. The full sorption-desorption cycle was therefore repeated on CIP/ARG using a maximum equilibration time of six hours, rather than the usual time of three hours. However, at the end of the study the mass of the sample was still significantly larger than its starting value (Fig. A.6, Supplementary Material). The plot of change in mass vs. time for this sample also showed that it did not remain at any RH stage for longer than 180 min, meaning that it had sufficient time to equilibrate fully. Therefore, this hysteresis is not due to inadequate equilibration time. A possible alternative explanation may be that the diffusion of water from the interior of these particles to the surface is significantly slower than water uptake, and therefore a portion of absorbed water remained in the sample at the end of the study [47].

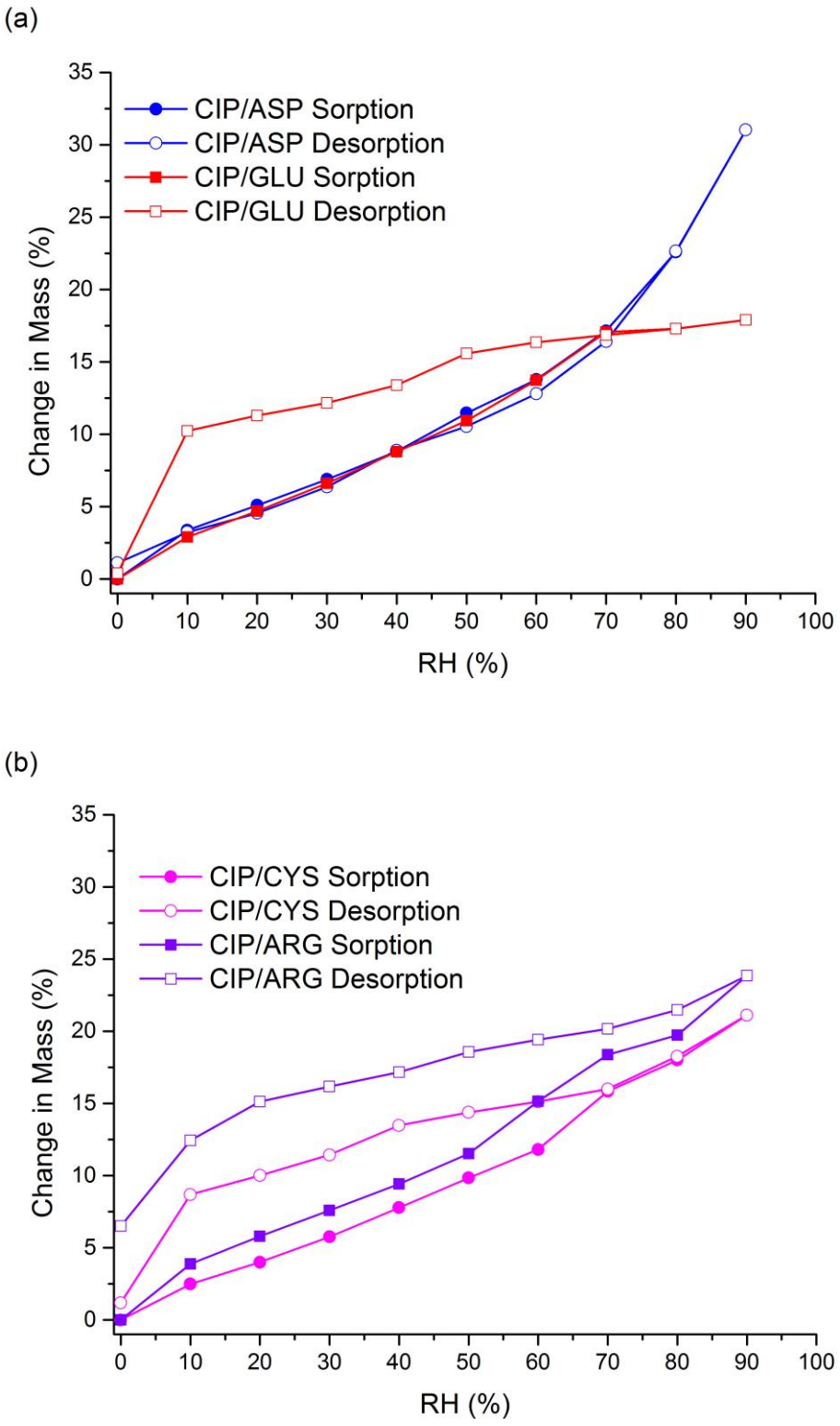


**Fig. 9.** DVS isotherms of CIP/amino acid ASDs: (a) CIP/ASP and CIP/GLU (b) CIP/CYS and CIP/ARG.

PXRD analysis at the end of the desorption cycle showed that all of the ASDs crystallized during the DVS study (Fig. A.7a, Supplementary Material). Absorbed water can act as a plasticizer for amorphous materials, increasing their molecular mobility and decreasing their $T_g$, leading to crystallization [48]. In contrast, CIP ASDs containing various acidic polymers as stabilizers remained X-ray amorphous following DVS analysis, and were also resistant to crystallization during DSC measurements [3]. The greater stability of these formulations may be attributed to the presence of polymers, which are known to hinder crystallization due their effects on molecular mobility, antiplasticization and steric hindrance [49]. The PXRD diffractograms obtained with the CIP/ARG, CIP/CYS and CIP/GLU ASDs matched those of the amino acid starting materials plus the CIP 3.7 hydrate [28]. In contrast, the PXRD pattern obtained with CIP/ASP at the end of the DVS experiment resembled that obtained by slow solvent evaporation of an ethanolic solution of CIP and ASP (Fig. 8b), with matching peaks at approximately 5.2, 26.1 and 27.3 2θ degrees. As discussed above, the product obtained from this slow crystallization process is believed to contain CIP aspartate, plus an unidentified phase, possibly a hydrate of this salt. Additional unidentified peaks were present at approximately 10.3, 13.8 and 20.0 2θ degrees in the diffractogram of CIP/ASP following DVS, which possibly may also correspond to a hydrate of CIP aspartate.

Crystallization during water sorption can usually be identified by weight loss, as the crystalline solid cannot retain all of the water absorbed by the amorphous material [50]. From the change in mass vs. time plots of these samples, it could be seen that the ASD containing ARG crystallized at 70% RH during the sorption stage, whereas the other ASDs crystallized at 60% RH (data not shown). PXRD was also carried out on the samples following these crystallization events to determine whether the phase that initially crystallized differs from that obtained at the end of the

study (Fig. A.7b, Supplementary Material). A similar PXRD pattern was obtained with the CIP/ARG ASD at both time points, although there were some differences in peak intensity. In the case of CIP/CYS, at 60% RH only small peaks corresponding to zwitterionic CIP and the CIP 3.7 hydrate could be identified. The drug therefore appears to crystallize at a lower RH level than the amino acid in these samples.

Although the PXRD patterns of CIP/ASP were quite similar at both time points, the sample that crystallized at 60% RH more closely matched that obtained when the ASD was allowed to crystallize slowly at RT via exposure to the air (Fig. 8c). Two crystallization events were detected with the CIP/GLU ASD, at 60% and 80% RH. Following the second crystallization the PXRD pattern was very similar to that obtained at the end of the desorption stage, but the peaks were of a higher intensity. At 60% RH however, the PXRD pattern of the sample was almost identical to that of CIP/ASP at the same RH level. The same pattern was also obtained when both of these ASDs were left exposed at RT for one week, during which time they would have experienced a similar temperature to that used in DVS analysis. As discussed above, the fact that very similar X-ray diffractograms were obtained with CIP/ASP and CIP/GLU upon RT crystallization of the ASDs may be due to the formation of isostructural CIP aspartate and CIP glutamate salts. Therefore, these ASDs appear to initially crystallize to their corresponding salts during the water sorption stage of DVS analysis. The glutamate salt then dissociates to the starting materials at higher RH levels, whereas CIP aspartate forms an additional unidentified phase, perhaps due to hydration of the salt. A summary of the major phases identified following crystallization of the ASDs during DSC and DVS analysis is presented in Fig. A.8, Supplementary Material.

As all of the ASDs crystallized when exposed to high humidity during DVS analysis, a long-term stability study was carried out under dry conditions at RT. All of the ASDs remained fully X-ray amorphous for 10 months under these storage conditions; however, at the 12 month time point a small peak was visible at 25.3 2θ degrees in the X-ray diffractogram of CIP/CYS, which corresponds to the most prominent PXRD peak of anhydrous zwitterionic CIP (Fig. A.9, Supplementary Material). This ASD would be expected to have the lowest stability of these samples due to its lower $T_g$. In addition, the fact that CIP/CYS crystallized to zwitterionic CIP during DSC and DVS analysis, whereas CIP/ASP and CIP/GLU appear to have formed the corresponding crystalline salts, indicates that the interactions between the drug and amino acid are somewhat weaker in the former formulation. The higher $T_g$'s obtained with the other ASDs suggests that CIP interacts more extensively with ASP, GLU and ARG, which would help to reduce the molecular mobility of the drug and increase the energy barrier to crystallization [51,52].

### 3.6. Dynamic Solubility Studies

The concentration of CIP obtained during solubility studies in water, FaSSIF and FaSSGF is shown in Fig. 10. Expanded sections of the plots are also shown for clarity. The samples behaved very similarly in water and FaSSIF. In each case the highest CIP concentration was obtained with the CIP/ASP ASD, which reached a maximum concentration of 49.6 ± 7.1 mg/mL and 44. 5 ± 3.0 mg/mL in each medium, respectively. This was followed by the CIP/GLU ASD, which attained 36.6 ± 2.1 mg/mL and 31.3 ± 0.5 mg/mL, respectively, in these media. The concentration of CIP increased rapidly with both ASDs in the first few minutes, and then

remained fairly constant for the duration of the study. The CIP salts prepared by Elshaer et al were also found to be highly soluble in water, with concentrations of 215±13.3 mg/mL and 185.4±8.6 mg/mL reportedly achieved after 12 hours with the glutamate and aspartate salts, respectively [14].

While the CIP/ASP and CIP/GLU PMs behaved similarly to the equivalent ASDs, a significantly higher concentration was obtained with the amorphous samples. This solubility advantage can be attributed to their solid state, i.e. formulation as an amorphous salt. However, high CIP concentrations of 20.3 ± 0.7 mg/mL and 16.9 ± 2.3 mg/mL were still obtained with the CIP/ASP and CIP/GLU PMs, respectively, in water. The ability of these PMs to increase the solubility of CIP may be explained by their effect on pH. The pH of 2% (w/v) solutions of the pure amino acids in water were therefore measured, which resulted in a pH of 2.9, 3.1, 4.7 and 11.6 with ASP, GLU, CYS and ARG, respectively. The solubility of CIP is greatly increased at low pH, as it bears a net positive charge. Therefore, a significant improvement in drug solubility would be expected for mixtures containing ASP and GLU. The pH of the solutions at the end of the solubility studies was also measured, and a comparison of these values is shown in Fig. 10d. Like other pharmaceutical salts, the amino acids most likely dissociate rapidly upon addition to solvent, altering the pH of the dissolution layer around the drug and increasing its solubility and dissolution rate [53]. As expected, the lowest final pH was obtained with the samples containing the acidic amino acids. Both the PMs and ASDs containing ASP and GLU had a pH of 4.4–4.9 at the end of the study, no matter what the original pH of the medium.

The ASDs containing CYS and ARG offered less of a solubility advantage than the acidic amino acids. Crystalline CIP has a low solubility of only 0.09 ± 0.0 mg/mL in water, whereas statistically significantly higher concentrations of 1.3 ± 0.3 mg/mL and 1.1 ± 0.04 mg/mL were

obtained with the CIP/CYS and CIP/ARG ASDs, respectively. Similar concentrations of 0.6–1.7 mg/mL were previously obtained with polymeric CIP ASDs containing Eudragit L100 and HPMCAS in water [3]. While the PM containing ARG was approximately 7 times more soluble than the pure drug in water, the CIP/CYS PM did not offer a significant advantage. The increased solubility of the former PM is most likely due to its effect on pH. At the end of the study the pH was found to be 9.6 for this PM, compared to 6.4 for CIP/CYS. This should result in a greater proportion of ionized CIP (in this case negatively charged), and thus higher drug solubility. In FaSSIF pure CIP reached a slightly higher concentration of approximately 0.14 mg/mL at the end of the study. As in water, a significantly higher concentration was obtained with the CIP/ARG and CIP/CYS ASDs, however they were substantially less soluble than the ASDs containing ASP and GLU, reaching only 0.5 ± 0.0 mg/mL and 0.3 ± 0.0 mg/mL, respectively. In contrast, the CIP/ARG PM did not differ significantly from the pure drug, and the CIP/CYS PM also had a low solubility of approximately 0.2 mg/mL. Therefore, the improved solubility of these ASDs compared to the PMs may be attributed to their amorphous nature. The polymeric CIP ASDs were somewhat more soluble in this medium, achieving final concentrations of 1.3–1.9 mg/mL [3], however they were still far less soluble than CIP/ASP and CIP/GLU.

A much higher concentration was obtained with all of the samples in FaSSGF compared to FaSSIF and water. While CIP has an overall neutral charge near pH 7, at pH 1.6 the drug is positively charged, and thus far more soluble. This enabled pure CIP to reach a concentration of 11.3 ± 0.2 mg/mL at the end of the study. Each ASD was more soluble than the equivalent PM at this pH, confirming the solubility advantage of the amorphous formulations. Again, the samples containing the acidic amino acids had the highest solubility, with the CIP/ASP and CIP/GLU

ASDs reaching concentrations of 240.1 ± 38.6 mg/mL and 120.4 ± 6.4 mg/mL, respectively. The solubility of the corresponding PMs was approximately 15 and 8 times greater than that of the crystalline drug, respectively. The CIP/CYS ASD and PM were also significantly more soluble in FaSSGF, reaching approximately 17.0 ± 0.4 mg/mL and 15.1 ± 1.6 mg/mL, respectively. In contrast, the solubility of the CIP/ARG ASD only increased modestly to 3.7 ± 0.2 mg/mL, which was significantly lower than the concentration achieved with pure crystalline CIP. Again, this may be explained by pH effects. While the samples containing ARG produced a basic pH in water, the lower starting pH of FaSSGF resulted in a more neutral overall pH of 5.1 upon dissolution of this ASD, and thus limited the solubility of CIP. Similarly, ASDs containing CIP and Eudragit L100 or HPMCAS were also found to significantly increase the solubility of CIP in water and FaSSIF, but to decrease it in FaSSGF to 3–4 mg/mL. This may be explained by the fact that the polymers present in these ASDs are insoluble in acidic media, which would have hindered the release of the drug [3]. As was the case with the other amino acids, the amorphous nature of the CIP/ARG ASD significantly improved its solubility in FaSSGF relative to the equivalent PM, which had a final concentration of only 0.18 ± 0.0 mg/mL.

(a)

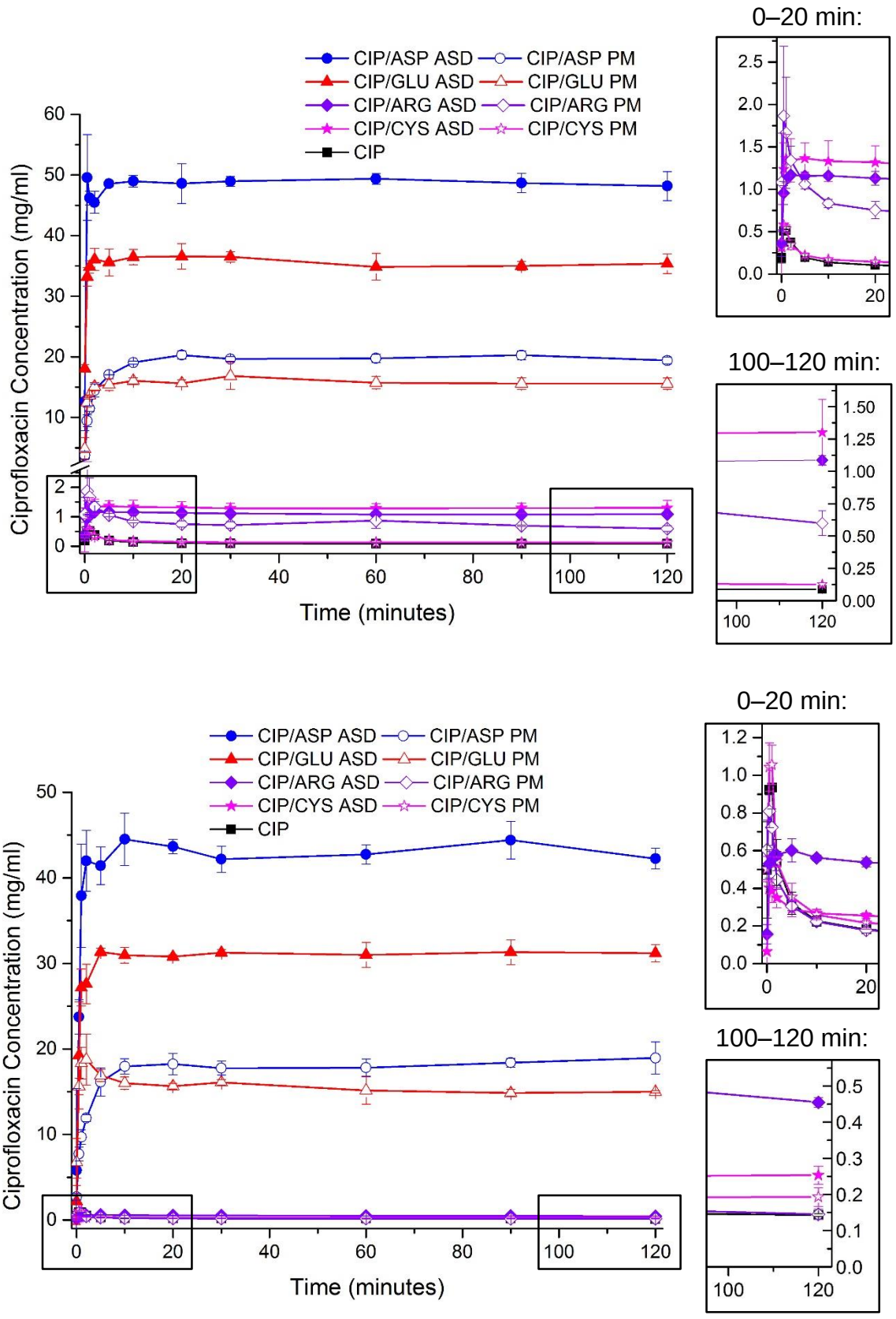
0–20 min:
100–120 min:
CIP/ASP ASD
CIP/ASP PM
CIP/GLU ASD
CIP/GLU PM
CIP/ARG ASD
CIP/ARG PM
CIP/CYS ASD
CIP/CYS PM
CIP
Ciprofloxacin Concentration (mg/ml)
Time (minutes)
0–20 min:
100–120 min:
CIP/ASP ASD
CIP/ASP PM
CIP/GLU ASD
CIP/GLU PM
CIP/ARG ASD
CIP/ARG PM
CIP/CYS ASD
CIP/CYS PM
CIP
Ciprofloxacin Concentration (mg/ml)
Time (minutes)

(c)

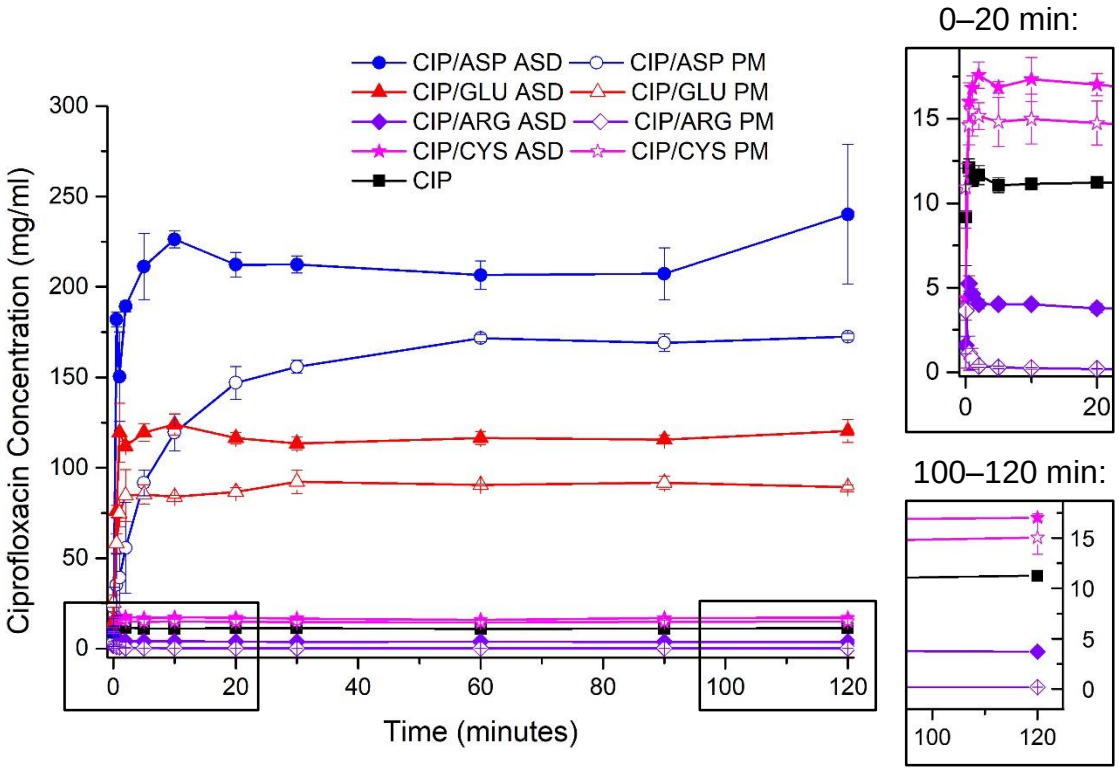
0–20 min:
100–120 min:
CIP/ASP ASD
CIP/ASP PM
CIP/GLU ASD
CIP/GLU PM
CIP/ARG ASD
CIP/ARG PM
CIP/CYS ASD
CIP/CYS PM
CIP
Ciprofloxacin Concentration (mg/ml)
Time (minutes)

(d)

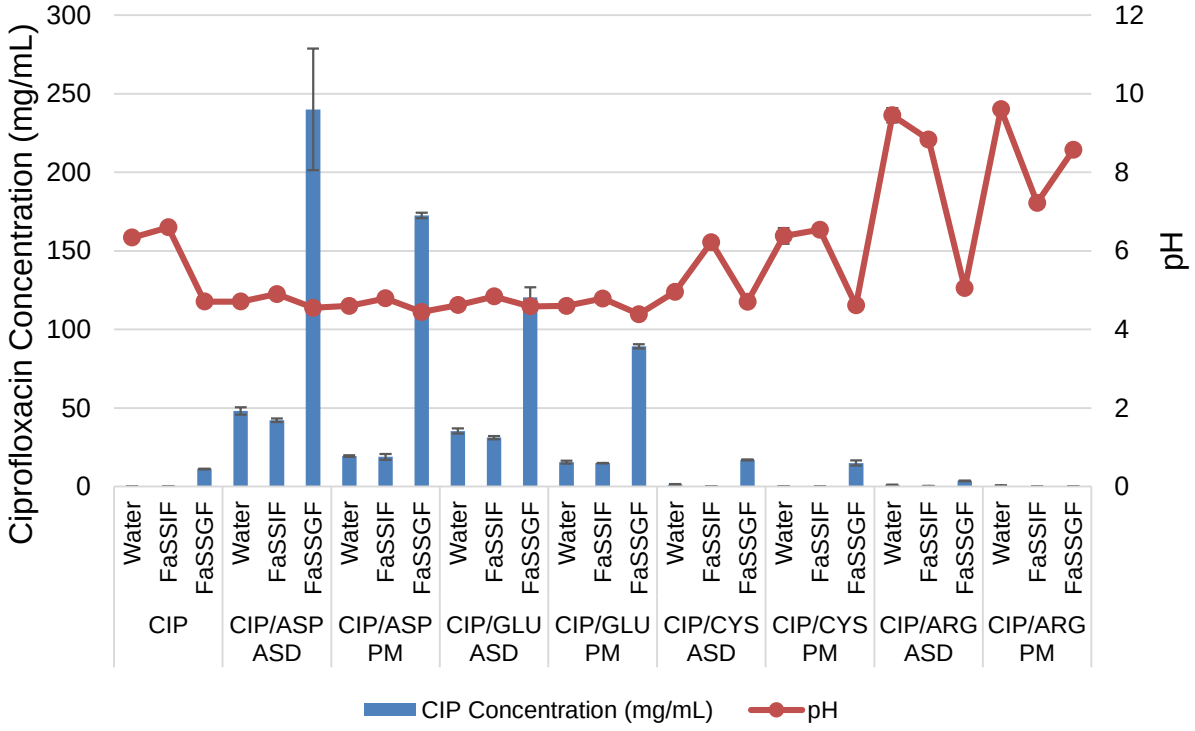
Ciprofloxacin Concentration (mg/mL)
pH
Water
FaSSIF
FaSSGF
CIP
CIP/ASP ASD
CIP/ASP PM
CIP/GLU ASD
CIP/GLU PM
CIP/CYS ASD
CIP/CYS PM
CIP/ARG ASD
CIP/ARG PM
CIP Concentration (mg/mL)
pH

**Fig. 10.** Solubility studies in (a) water (b) FaSSIF and (c) FaSSGF at 37 ºC. The panels on the right show enlarged sections of the plots. (d) Concentration and pH of solutions at end of solubility studies. The average of at least 3 experiments is plotted, ± the standard deviation (represented by the error bars).

PXRD analysis of the solid residues left at the end of the solubility studies showed that all of the samples crystallized in each solvent (Fig. A.10, Supplementary Material). In each case, less intense PXRD peaks were obtained with the ASDs than the PMs. With pure CIP the 3.1 hydrate was detected following solubility studies in water, while the 3.7 hydrate forms in FaSSIF and FaSSGF [3]. The CIP 3.7 hydrate also crystallized from all of the samples containing CYS and ARG, the CIP/GLU and CIP/ASP ASDs and CIP/GLU PM in FaSSIF, and the CIP/ASP ASD and PM in water. The PXRD patterns of the remaining ASP and GLU ASDs and PMs on the other hand matched that of the CIP 3.1 hydrate.

In order to confirm that the solubility advantage of the ASDs was not purely due to their effect on pH, a theoretical pH-solubility profile was constructed for pure crystalline CIP using a modification of the Henderson-Hasselbalch equation:

$$S_T = [B]\,(1 + 10^{pKa1-pH} + 10^{pH-pKa2}) \quad (2)$$

$S_T$ is the total solubility of the drug in moles/L. [B] is the concentration of the free base, which is equal to approximately 0.000266 M for CIP. As previously mentioned, the $pK_a$ of the carboxylic acid ($pK_{a1}$) and piperazine amine ($pK_{a2}$) of CIP are equal to 6.16 and 8.62, respectively [25]. The

theoretical pH-solubility profile of the commercial hydrochloride salt, CIP HCl, was also included for comparison.

As can be seen from Fig. 11, the experimental solubility data did not fit the theoretical pH-solubility curve of CIP exactly. The solubility of the pure drug in FaSSGF is higher than predicted, and aligns more closely with the CIP HCl curve, due to the presence of HCl in this media. The experimental data points obtained in water with the ASDs and PMs containing ARG and CYS align quite well with the theoretical curve of CIP, whereas in FaSSIF they displayed slightly higher than predicted solubilities. This may be due to the presence of surfactants in this medium, which should improve the solubility of the drug via solubilization. Both of these ASDs were more soluble than the equivalent PMs in all media. This suggests that the solid state changes introduced by ball milling contributed to their improved solubility. Like the pure drug, the solubility of these samples was increased in FaSSGF, so that the data points lay closer to the CIP HCl curve. The CIP/ASP and CIP/GLU PMs also behaved similarly to CIP HCl in water and FaSSIF. In FaSSGF the combination of an acidic counterion and low pH medium enabled an even larger amount of drug to enter solution from these samples. However, with the corresponding ASDs, a greater divergence from the theoretical pH-solubility plot was observed. Therefore, while pH certainly plays a part in the solubility enhancement of these samples, their disordered nature resulted in an additional increase in solubility in each case.

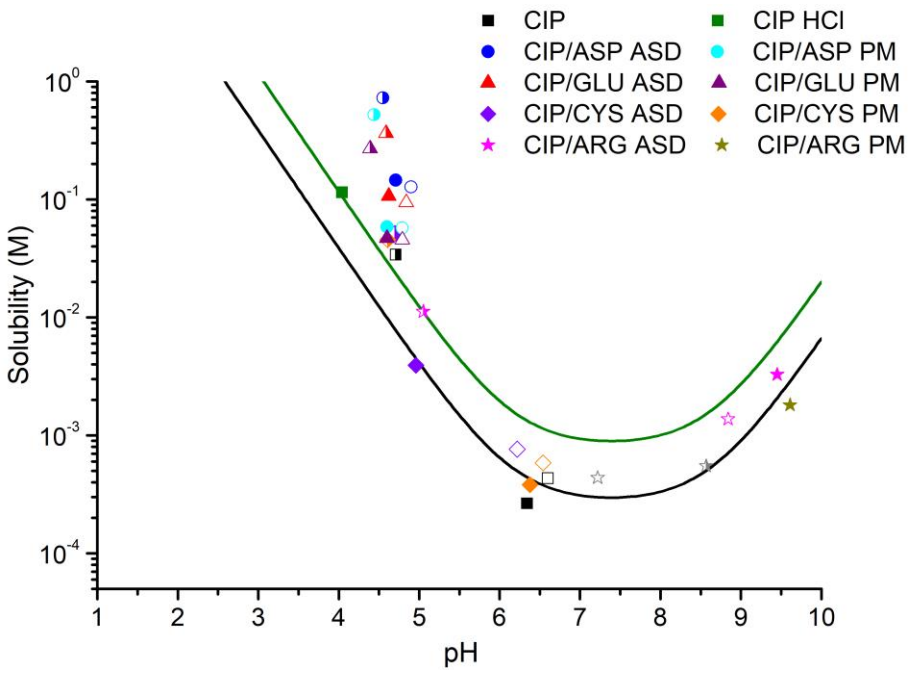


**Fig. 11.** Theoretical pH-solubility profiles of CIP (black) and CIP HCl (green). The symbols represent the average concentrations obtained from solubility studies after two hours in water (filled symbols), FaSSIF (empty symbols) and FaSSGF (half-filled symbols).

### 3.7. PAMPA Permeability Study

The results of the PAMPA study on CIP and the CIP/amino acid ASDs are shown in Table 4. The commercially available salt, crystalline ciprofloxacin hydrochloride (CIP HCl), was also examined for comparison. All of the samples had an effective permeability ($P_e$) value less than 1 x $10^{-6}$ cm/s, and can therefore be described as poorly permeable [54]. CIP from its hydrochloride salt, CIP/GLU and CIP/ASP had the lowest permeability, however they were not statistically significantly different from each other, as shown by Tukey's multiple comparison test. The drug from CIP/CYS had the highest average permeability, followed by that from CIP/ARG, however

these samples also did not differ significantly from each other. Individual two-sample *t* tests were used to compare the $P_e$ value of crystalline CIP to those of the ASDs and CIP HCl. In each case a statistically significant difference was obtained (see *p*-values in Table 4). With CIP/ASP, CIP/GLU and CIP HCl, a significant decrease in $P_e$ was seen, whereas a significant increase was observed with CIP/CYS and CIP/ARG.

**Table 4**. PAMPA Permeability Values of CIP

| **Sample** | **$P_e$[a] x $10^6$ (cm/s)** | ***p*-value[b]** |
|---|---|---|
| CIP | 0.56 ± 0.06 | N/A |
| CIP HCl | 0.32 ± 0.00 | 0.00 |
| CIP/ASP | 0.38 ± 0.05 | 0.02 |
| CIP/GLU | 0.31 ± 0.01 | 0.00 |
| CIP/CYS | 0.87 ± 0.15 | 0.03 |
| CIP/ARG | 0.73 ± 0.04 | 0.02 |

[a]$P_e$: effective permeability. The average of three measurements is shown, ± the standard deviation. [b]*p*-value from *t* test comparing $P_e$ of CIP with those of the other samples.

The poor permeability of pure CIP may be explained by the fact that the drug primarily exists as the zwitterion at neutral pH [55]. While the unionized form of the drug can enter and diffuse across lipid membranes relatively easily, this is not the case for the zwitterion.[56] In aqueous solutions, groups of zwitterionic CIP molecules interact "head-to tail", resulting in a decrease in their electrostatic potential. These stacks are further stabilized by hydrogen bonding with water molecules, making it unlikely that they will be undergo passive transmembrane transport [56]. However, it is believed that a portion of zwitterionic CIP transforms to the unionized form in the vicinity of cell membranes due to proton transfer [25], enabling passive diffusion of the drug.

The lower permeability of CIP from the hydrochloride salt, CIP/ASP and CIP/GLU may be attributed to their acidic counterions. The presence of these acidic compounds in solution will increase the proportion of positively charged CIP, making the drug more soluble, but decreasing its lipophilicity. The octanol/water partitioning of CIP has also been found to decrease when ASP or GLU are dissolved in the aqueous phase [57]. Such a trade-off between increased solubility and decreased permeability is a common issue with solubility-enhancing formulations [58]. In contrast, CYS and ARG do not appear to greatly increase the proportion of ionized CIP in solution, and therefore the formulation of CIP as an ASD with these amino acids did not decrease its permeability. This was also true for the polymeric CIP ASDs examined in a previous study. While the ASDs containing Eudragit L100 and HPMCAS-MG did not significantly alter the permeability of CIP, the CIP from the HPMCAS-LG ASD was statistically significantly more permeable than the pure crystalline drug, with a $P_e$ of $0.75 \pm 0.06 \times 10^{-6}$ cm/s, comparable to that of CIP from CIP/ARG and CIP/CYS [3].

Due to its simplicity, the PAMPA model only estimates passive transcellular drug absorption. However, the zwitterionic form of CIP can also be absorbed via the paracellular pathway by passing through water-filled channels in-between intestinal cells, and it has been calculated that 18% of CIP is transported in this manner [59]. As the tight junctions in-between epithelial cells are believed to be selective for positively charged molecules [60], the cationic form of CIP should be able to cross the intestinal barrier relatively easily via the paracellular route. Therefore, the total *in vivo* absorption of these samples, in particular the ASDs containing ASP and GLU, is likely to be somewhat higher than that estimated here. This may explain the results of Elshaer et al's study in Caco-2 cells, which found the permeability of their CIP/ASP and CIP/GLU salts to be slightly higher than that of CIP, which was reported as $0.8 \times 10^{-6}$ cm/s after 60 min. However,

this difference was not statistically significant in either case [57]. As the tight junctions present in Caco-2 cells are believed to be less permeable than those found in the epithelium of the small intestine [61], greater permeability enhancement could be expected with these salts *in vivo*. However, a good correlation between the results of PAMPA, Caco-2 and *in vivo* rat in-situ permeability studies has been found for CIP [25], and therefore PAMPA is a suitable method for quickly comparing the permeability of the ASDs to that of the pure drug.

## 4. Conclusions

This study demonstrated that certain amino acids may be used as stabilizers for amorphous formulations containing the poor glass-forming zwitterionic drug CIP. ASP, GLU, CYS and ARG were successful in this regard, and in each case FTIR and SSNMR confirmed the formation of an amorphous salt between the positively charged piperazine amino group of CIP and the negatively charged α-carboxylate groups of the amino acids. These salts remained fully X-ray amorphous for at least 10 months when stored under dry conditions, although after 12 months CIP/CYS showed some evidence of crystallization. In contrast, all of the ASDs crystallized during DSC and DVS studies, making them less stable than the binary polymeric CIP ASDs produced previously.

Significant improvements in the solubility of CIP were seen with all of the ASDs. In each case the ASDs were significantly more soluble than the corresponding physical mixtures, confirming that their amorphous state offers an additional boost in solubility. However, a trade-off between the solubility and permeability of the samples was observed. While the ASDs containing ASP and GLU offered the greatest solubility enhancement, they were also significantly less permeable

than pure crystalline CIP, as the acidic counterions induce protonation of the drug. In contrast, CIP/CYS and CIP/ARG significantly improved the permeability of CIP, but had a much more modest effect on its solubility compared to CIP/ASP and CIP/GLU. Similar results have been obtained in a previous study, whereby the solubility and permeability of ball milled ASDs consisting of CIP and HPMCAS were on par with those of CIP/CYS and CIP/ARG. Due to their greater solubility-permeability balance, the ASDs containing CYS, ARG and HPMCAS may be the most promising in terms of bioavailability enhancement of CIP, although the particularly high solubility of CIP/ASP and CIP/GLU may help to offset their lower permeability. However, further studies, with more representative permeability models, would be necessary to determine whether any of these samples provide a true benefit *in vivo*.

**Acknowledgements**

Funding for this research was provided by the Science Foundation Ireland under grant No. 12/RC/2275 (Synthesis and Solid State Pharmaceutical Centre). The authors wish to acknowledge Andrea Burke for her assistance in solubility studies.

**References**

[1] S.A. Breda, A.F. Jimenez-Kairuz, R.H. Manzo, M.E. Olivera, Solubility behavior and biopharmaceutical classification of novel high-solubility ciprofloxacin and norfloxacin pharmaceutical derivatives, Int. J. Pharm. 371 (2009) 106–13.

[2] H. Mesallati, N.A. Mugheirbi, L. Tajber, Two faces of ciprofloxacin: investigation of proton

transfer in solid state transformations, Cryst. Growth Des. 16 (2016) 6574–85.

[3] H. Mesallati, A. Umerska, K. Paluch, L. Tajber, Amorphous polymeric drug salts as ionic solid dispersion forms of ciprofloxacin, Mol. Pharm. 14 (2017) 2209–2223.

[4] N.M. Zaki, P. Artursson, C.A.S. Bergström, A modified physiological BCS for prediction of intestinal absorption in drug discovery, Mol. Pharm. 7 (2010) 1478–87.

[5] S.J. Dengale, H. Grohganz, T. Rades, K. Löbmann, Recent advances in co-amorphous drug formulations, Adv. Drug Deliv. Rev. 100 (2016) 116–125.

[6] K.J. Paluch, T. McCabe, H. Müller-Bunz, O.I. Corrigan, A.M. Healy, L. Tajber, Formation and physicochemical properties of crystalline and amorphous salts with different stoichiometries formed between ciprofloxacin and succinic acid, Mol. Pharm. 10 (2013) 3640–54.

[7] A. Tilborg, B. Norberg, J. Wouters, Pharmaceutical salts and cocrystals involving amino acids: a brief structural overview of the state-of-art, Eur. J. Med. Chem. 74 (2014) 411–26.

[8] K. Löbmann, H. Grohganz, R. Laitinen, C. Strachan, T. Rades, Amino acids as co-amorphous stabilizers for poorly water soluble drugs--Part 1: preparation, stability and dissolution enhancement, Eur. J. Pharm. Biopharm. 85 (2013) 873–81.

[9] K.T. Jensen, L.I. Blaabjerg, E. Lenz, A. Bohr, H. Grohganz, P. Kleinebudde, T. Rades, K. Löbmann, Preparation and characterization of spray-dried co-amorphous drug-amino acid salts, J. Pharm. Pharmacol. 68 (2016) 615–24.

[10] K.T. Jensen, K. Löbmann, T. Rades, H. Grohganz, Improving co-amorphous drug formulations by the addition of the highly water soluble amino acid, proline, Pharmaceutics.

6 (2014) 416–35.

[11] R. Laitinen, K. Loebmann, H. Grohganz, C. Strachan, T. Rades, Amino acids as co-amorphous excipients for simvastatin and glibenclamide: physical properties and stability, Mol. Pharm. 11 (2014) 2381–9.

[12] K.T. Jensen, F.H. Larsen, K. Löbmann, T. Rades, H. Grohganz, Influence of variation in molar ratio on co-amorphous drug-amino acid systems, Eur. J. Pharm. Biopharm. 107 (2016) 32–9.

[13] J.R. Patel, R.A. Carlton, F. Yuniatine, T.E. Needham, L. Wu, F.G. Vogt, Preparation and structural characterization of amorphous spray-dried dispersions of tenoxicam with enhanced dissolution, J. Pharm. Sci. 101 (2012) 641–63.

[14] A. ElShaer, D. Ouyang, P. Hanson, A.R. Mohammed, Preparation and evaluation of amino acid based salt forms of model zwitterionic drug ciprofloxacin, Pharm. Drug Deliv. Res. 2 (2013) 1–10.

[15] A.T. Heikkinen, L. DeClerck, K. Löbmann, H. Grohganz, T. Rades, R. Laitinen, Dissolution properties of co-amorphous drug-amino acid formulations in buffer and biorelevant media, Pharmazie. 70 (2015) 452–7.

[16] A. Dahan, J.M. Miller, The solubility-permeability interplay and its implications in formulation design and development for poorly soluble drugs, AAPS J. 14 (2012) 244–51.

[17] C.R. Morcombe, K.W. Zilm, Chemical shift referencing in MAS solid state NMR, J. Magn. Reson. 162 (2003) 479–86.

[18] B.M. Fung, A.K. Khitrin, K. Ermolaev, An improved broadband decoupling sequence for

liquid crystals and solids, J. Magn. Reson. 142 (2000) 97–101.

[19] F. Wohnsland, B. Faller, High-throughput permeability pH profile and high-throughput alkane/water log P with artificial membranes, J. Med. Chem. 44 (2001) 923–930.

[20] Merck Millipore, Lipid-PAMPA with the MultiScreen® filter plates, Billerica, MA, 2004.

[21] N.S. Trasi, S.R. Byrn, Mechanically induced amorphization of drugs: a study of the thermal behavior of cryomilled compounds, AAPS PharmSciTech. 13 (2012) 772–84.

[22] M. Mattern, G. Winter, U. Kohnert, G. Lee, Formulation of proteins in vacuum-dried glasses. II. Process and storage stability in sugar-free amino acid systems, Pharm. Dev. Technol. 4 (1999) 199–208.

[23] N. Chieng, J. Aaltonen, D. Saville, T. Rades, Physical characterization and stability of amorphous indomethacin and ranitidine hydrochloride binary systems prepared by mechanical activation, Eur. J. Pharm. Biopharm. 71 (2009) 47–54.

[24] G. Kasten, H. Grohganz, T. Rades, K. Löbmann, Development of a screening method for co-amorphous formulations of drugs and amino acids, Eur. J. Pharm. Sci. 95 (2016) 28–35.

[25] M. Bermejo, A. Avdeef, A. Ruiz, R. Nalda, J.A. Ruell, O. Tsinman, I. González, C. Fernández, G. Sánchez, T.M. Garrigues, V. Merino, PAMPA--a drug absorption in vitro model 7. Comparing rat in situ, Caco-2, and PAMPA permeability of fluoroquinolones, Eur. J. Pharm. Sci. 21 (2004) 429–41.

[26] J.M. Berg, J.L. Tymoczko, L. Stryer, Appendix: acid-base concepts, in: Biochemistry, 5th ed., W H Freeman, New York, 2002.

[27] V.L. Dorofeev, The betainelike structure and infrared spectra of drugs of the fluoroquinolone group, Pharm. Chem. J. 38 (2004) 698–702.

[28] L. Mafra, S.M. Santos, R. Siegel, I. Alves, F.A.A. Paz, D. Dudenko, H.W. Spiess, Packing interactions in hydrated and anhydrous forms of the antibiotic ciprofloxacin: a solid-state NMR, X-ray diffraction, and computer simulation study, J. Am. Chem. Soc. 134 (2012) 71–4.

[29] Y. Wang, D. Wilson, G.S. Harbison, Solid-State NMR and the crystallization of aspartic and glutamic acids, Cryst. Growth Des. 16 (2016) 625–31.

[30] A. Abraham, E. Mihaliuk, B. Kumar, J. Legleiter, T. Gullion, Solid-state NMR study of cysteine on gold nanoparticles, J. Phys. Chem. C. 114 (2010) 18109–14.

[31] J.-B. Guilbaud, H. Baker, B.C. Clark, E. Meehan, Y.Z. Khimyak, Effect of encapsulating arginine containing molecules on PLGA: a solid-state NMR study, J. Pharm. Sci. 99 (2010) 2697–710.

[32] J.W. Lubach, D. Xu, B.E. Segmuller, E.J. Munson, Investigation of the effects of pharmaceutical processing upon solid-state NMR relaxation times and implications to solid-state formulation stability, J. Pharm. Sci. 96 (2007) 777–787.

[33] A. Gunnam, K. Suresh, R. Ganduri, A. Nangia, Crystal engineering of a zwitterionic drug to neutral cocrystals: a general solution for floxacins, Chem. Commun. 52 (2016) 12610–13.

[34] C.B. Romañuk, R.H. Manzo, Y.G. Linck, A.K. Chattah, G.A. Monti, M.E. Olivera, Characterization of the solubility and solid-state properties of saccharin salts of

fluoroquinolones, J. Pharm. Sci. 98 (2009) 3788–801.

[35] K.-I. Izutsu, Y. Fujimaki, A. Kuwabara, N. Aoyagi, Effect of counterions on the physical properties of l-arginine in frozen solutions and freeze-dried solids, Int. J. Pharm. 301 (2005) 161–9.

[36] F. AlHusban, Y. Perrie, A.R. Mohammed, Formulation and characterisation of lyophilised rapid disintegrating tablets using amino acids as matrix forming agents, Eur. J. Pharm. Biopharm. 75 (2010) 254–262.

[37] T. Suzuki, F. Franks, Solid–liquid phase transitions and amorphous states in ternary sucrose–glycine–water systems, J. Chem. Soc., Faraday Trans. 89 (1993) 3283–3288.

[38] T.-C. Hua, B.-L. Liu, H. Zhang, Amino-acid type protective agents, in: Free. Pharm. Food Prod., Woodhead Publishing Limited, Cambridge, UK, 2010: p. 176.

[39] P. Gabbott, P. Clarke, T. Mann, P. Royall, S. Shergill, A high-sensitivity, sigh-speed DSC technique: measurement of amorphous lactose, (2014). http://www.perkinelmer.com/CMSResources/Images/44-157513APP_Measurement_Amorphous_Lactose_High-Sensitivity_High-Speed_DSC_Technique_010058_01.pdf (accessed August 13, 2015).

[40] N.S. Trasi, S.X.M. Boerrigter, S.R. Byrn, Investigation of the milling-induced thermal behavior of crystalline and amorphous griseofulvin, Pharm. Res. 27 (2010) 1377–89.

[41] M. Saunders, K. Podluii, S. Shergill, G. Buckton, P. Royall, The potential of high speed DSC (hyper-DSC) for the detection and quantification of small amounts of amorphous content in predominantly crystalline samples, Int. J. Pharm. 274 (2004) 35–40.

[42] J. Galcera, E. Molins, Effect of the counterion on the solubility of isostructural pharmaceutical lamotrigine salts, Cryst. Growth Des. 9 (2009) 327–334.

[43] S. Gaisford, A.B.M. Buanz, Pharmaceutical physical form characterisation with fast (>200 °C min−1) DSC heating rates, J. Therm. Anal. Calorim. 106 (2011) 221–6.

[44] B.C. Hancock, G. Zografi, Characteristics and significance of the amorphous state in pharmaceutical systems, J. Pharm. Sci. 86 (1997) 1–12.

[45] G. Zografi, States of water associated with solids, Drug Dev. Ind. Pharm. 14 (1988) 1905–26.

[46] S. Sheokand, S.R. Modi, A.K. Bansal, Dynamic vapor sorption as a tool for characterization and quantification of amorphous content in predominantly crystalline materials, J. Pharm. Sci. 103 (2014) 3364–76.

[47] A.S. Barham, F. Tewes, A.M. Healy, Moisture diffusion and permeability characteristics of hydroxypropylmethylcellulose and hard gelatin capsules, Int. J. Pharm. 478 (2015) 796–803.

[48] V. Andronis, M. Yoshioka, G. Zografi, Effects of sorbed water on the crystallization of indomethacin from the amorphous state, J. Pharm. Sci. 86 (1997) 346–51.

[49] J. Knapik, Z. Wojnarowska, K. Grzybowska, L. Tajber, H. Mesallati, K.J. Paluch, M. Paluch, Molecular dynamics and physical stability of amorphous nimesulide drug and its binary drug–polymer systems, Mol. Pharm. 13 (2016) 1937–1946.

[50] R. Surana, A. Pyne, R. Suryanarayanan, Effect of preparation method on physical properties of amorphous trehalose, Pharm. Res. 21 (2004) 1167–76.

[51] S.L. Shamblin, G. Zografi, The effects of absorbed water on the properties of amorphous mixtures containing sucrose, Pharm. Res. 16 (1999) 1119–24.

[52] J. Yang, K. Grey, J. Doney, An improved kinetics approach to describe the physical stability of amorphous solid dispersions, Int. J. Pharm. 384 (2010) 24–31.

[53] S.M. Berge, L.D. Bighley, D.C. Monkhouse, Pharmaceutical salts, J. Pharm. Sci. 66 (1977) 1–19.

[54] K. Sugano, Permeability of a drug, in: Biopharm. Model. Simulations Theory, Pract. Methods, Appl., 1st ed., John Wiley & Sons, New Jersey, 2012: p. 170.

[55] J. Sun, S. Sakai, Y. Tauchi, Y. Deguchi, J. Chen, R. Zhang, K. Morimoto, Determination of lipophilicity of two quinolone antibacterials, ciprofloxacin and grepafloxacin, in the protonation equilibrium, Eur. J. Pharm. Biopharm. 54 (2002) 51–8.

[56] O. Cramariuc, T. Rog, M. Javanainen, L. Monticelli, A. V Polishchuk, I. Vattulainen, Mechanism for translocation of fluoroquinolones across lipid membranes, Biochim. Biophys. Acta. 1818 (2012) 2563–71.

[57] A. Elshaer, Amino acids in oral drug delivery: salts, ion-pairs and transcriptomics, Aston University, 2013.

[58] J.M. Miller, A. Beig, R.A. Carr, J.K. Spence, A. Dahan, A win-win solution in oral delivery of lipophilic drugs: supersaturation via amorphous solid dispersions increases apparent solubility without sacrifice of intestinal membrane permeability, Mol. Pharm. 9 (2012) 2009–16.

[59] K.Y. Tam, A. Avdeef, O. Tsinman, N. Sun, The permeation of amphoteric drugs through

artificial membranes--an in combo absorption model based on paracellular and transmembrane permeability, J. Med. Chem. 53 (2010) 392–401.

[60] D.W. Powell, Barrier function of epithelia, Am. J. Physiol. 241 (1981) G275-88.

[61] P. Artursson, A.L. Ungell, J.E. Löfroth, Selective paracellular permeability in two models of intestinal absorption: cultured monolayers of human intestinal epithelial cells and rat intestinal segments., Pharm. Res. 10 (1993) 1123–9.